Astral microtubule dynamics regulate anaphase oscillation onset and set a robust final position for the *Caenorhabditis elegans* zygote spindle

Hélène Bouvrais,[1,2,*] Laurent Chesneau,[1,2] Sylvain Pastezeur,[1,2] Marie Delattre,[3] and Jacques Pécréaux[1,2,*]

Affiliations

[1]CNRS UMR 6290, F-35043 Rennes, France.

[2]University of Rennes 1, UEB, SFR Biosit, School of Medicine, F-35043 Rennes, France

[3]Laboratory of Molecular Biology of the Cell, École Normale Supérieure de Lyon, CNRS, F-69364 Lyon, France

Correspondence: helene.bouvrais@univ-rennes1.fr; jacques.pecreaux@univ-rennes1.fr (Lead Contact)

Graphical abstract

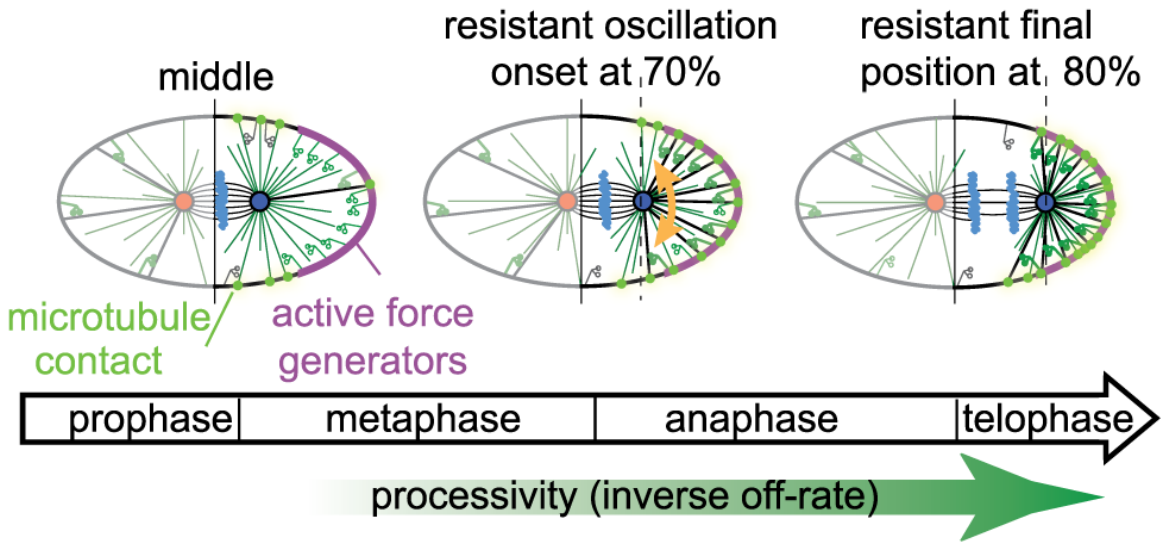

Abstract

Background: During asymmetric division of the *Caenorhabditis elegans* nematode zygote, the polarity cues distribution and daughter cell fates depend on the correct positioning of the mitotic spindle which results from both centering and cortical pulling forces. Revealed by spindle rocking, these pulling forces are regulated by the force generator dynamics, which are related to mitosis progression. This may be combined with a second regulation, this one by the posterior spindle pole position, which can be seen when comparing related species. **Results:** After delaying anaphase onset, we identified a positional pulling force regulation in *C. elegans*, which we ascribed to microtubule dynamics at the cortex. Indeed, in mapping the contacts we found a correlation between the centrosome–cortex distance and the microtubule contact density. This density in turn modulates pulling force generator activity. We expanded our model of spindle rocking and predicted then experimentally validated that the oscillation onset position resists changes in cellular geometry and number of force generators. Consistent with final spindle position measurements, this new model accounts for a lower dependence on force generator dynamics and quantities than predicted by the previous model. **Conclusion:** The spindle position regulates the rapid increase in forces needed for anaphase oscillation and positioning through the spatial modulation of microtubule-cortex contacts. This regulation superimposes that of force generator processivity, putatively linked to the cell cycle. This novel control confers resistance to variations in zygote geometry and dynamics of cortical force generators. Interestingly, this robustness originates in cell mechanics rather than biochemical networks.

Highlights

- Microtubule contacts at the cortex concentrate in regions close to the centrosomes.
- This regulates pulling forces and creates a positional switch on oscillation onset.
- The onset position resists changes in embryo length and force generator dynamics.
- The final centrosome position resists changes in generator quantities and dynamics.

Asymmetric cell divisions, with their differing daughter cell sizes, contents, and fates, are essential to the development of multicellular organisms[1,2]. As with many other species[3,4], the mitotic spindle helps position the cytokinesis cleavage furrow in the nematode *Caenorhabditis elegans*[5]. To correspond to cortical polarity cues, the spindle needs to be oriented along the polarity axis[6] and displaced out of the cell centre before cytokinesis[6,7]. Most asymmetric division includes pulling forces from the cell cortex that are exerted on the astral microtubule plus ends, and these forces are key in positioning and orienting the spindle[6,7,8].

In the one-cell nematode embryo, cortical forces are generated by a well-conserved trimeric complex which pulls on astral microtubules. The complex is made up of a dynein/dynactin complex, a LIN-5 NuMA homolog, and the G-protein regulators GPR-1/2, which are mammalian LGN homologs[9]. In an asymmetric division, GPR-1/2 reflect polarity cues[10] through their asymmetric locations[11,12], increasing the number of local active force generators[10,13]. During the centring phase[14], GPR-1/2 help orient the spindle along the anteroposterior axis (AP axis). They also aid in "overcentration," the displacement of the pronuclei centrosome complex (PCC) from the posterior side of the embryo to a slightly anterior position[12,15]. During prometaphase and metaphase, the spindle is maintained in the middle by centring forces that are independent of GPR-1/2 and may be caused by microtubule pushing on the cell cortex[16]. GPR-1/2-dependent cortical pulling forces become dominant in late metaphase and anaphase, displacing the spindle posteriorly, rocking it, and contributing to its elongation[17,18,19].

The activity of the cortical force generators is regulated in three different ways. The first is in space, through variation in *active* force generator counts across the distinct cortical regions in response to polarity cues. Twice as many force generators are active in the posterior cortex, where the PAR-2 polarity protein is present, than in the anterior one[10,17,20]. However, this active region only goes from 70% of the AP axis to the posterior tip of the embryo. This is because the LET-99 protein inhibits the GPR-1/2 location in the middle region (40 to 70% of the AP axis)[21,22]. Secondly, the number of active force generators is regulated in time, as it increases during cell division[18], likely according to mitotic progression[23]. Spindle rocking and posterior displacement can be explained by an anaphase-wide decrease in the force generator microtubule off-rate, which results in an increase in the overall pulling force[19] (Supplementary Text 2.2.1). In a third type of regulation, microtubule dynamics can also regulate cortical pulling forces[24]. Our initial "tug-of-war" physical model assumed that astral microtubules were abundant at the cortex during anaphase, and that the only limiting factor was the binding/unbinding dynamics of the force generators. However, such an abundance of microtubules, likely to occur during anaphase, is questionable in earlier phases. Indeed, Kozlowski et al. proposed a model in which limited microtubule access to the cortex accounts for spindle oscillation[25]. In addition, the duration of microtubule contacts at the cell cortex appears to be different on the anterior and posterior sides of the embryo[24]. Thus microtubule dynamics could regulate in another way, increasing the number of active force generators along the course of the cell division[26].

Previous studies have emphasized the key role of microtubules in the positioning of the microtubule-organizing centre (MTOC). Indeed, they can "sense" cell geometry, for example to bring the MTOC to the cell centre[27,28], or to orient the nucleus by exerting pulling forces that scale with microtubule length[29]. Similarly, in HeLa cells, microtubules "integrate" the adhesive pattern, whose cues are cortical, to orient the spindle accordingly[30]. In the *C. elegans* embryo, microtubules may contribute the orientation of the spindle by combining oblong embryo shape with polarity cues[31]. We therefore wondered whether the different microtubule contact densities in various regions of the cortex would modulate cortical force generation.

We recently observed in *Caenorhabditis briggsae* that both anaphase spindle oscillation onset and thus pulling forces are controlled by the position of the posterior spindle pole rather than by mitosis progression. In fact, oscillations start when the posterior pole reaches 70% of the AP axis in two nematode species (*C. elegans* and *C. briggsae*) which diverged 100 million years ago. Interestingly, in *C. briggsae,* this position was reached 30 seconds after anaphase onset but simultaneously to this onset in *C. elegans*. Taking into account the fact that GPR-1/2 levels are key to the regulation of cortical pulling forces[10,17], this robust oscillation onset is even more striking, since GPR is duplicated in *C. elegans* and because the GPR sequences are different in the two species[12]. These observations suggest that a positional switch controls pulling forces, and we propose here that this switch has to do with microtubule dynamics.

Measuring the residency time of microtubules at the cell cortex throughout mitosis was key to exploring our hypothesis. While the microtubule dynamics in the cytoplasm over time are quite clear in nematode embryos[26], the time spent at the cortex is less well understood, with published values ranging from 1 to more than 10 seconds[24,25]. This discrepancy can be explained by the accelerated dynamics of microtubules, which requires high frame rate imaging. In this paper, we carefully measured the spatial variation of such dynamics. We used the results to decipher the regulatory role of microtubule dynamics on cortical pulling forces, thus accounting for the decoupling between oscillation and anaphase onsets observed in *C. briggsae*[12] and in *C. elegans*. Our initial tug–of–war model, focused on force generator dynamics, was expanded to encompass this cortical pulling force positional switch. We challenged the new model, comparing the switch's predicted and experimental resistances to both embryo shape variation and displacing of the active force generator region boundaries. Investigating the posterior displacement and using an *in silico* approach, we explored the consequences of this novel regulation of the spindle's final position, which itself contributes to cleavage furrow positioning.

Results

Spindle oscillations can start before anaphase onset in *C. elegans*.

We previously reported that the position of the spindle's posterior pole controls the onset of spindle oscillation in *C. briggsae*[12]. We wondered whether the simultaneous onsets of anaphase and oscillation seen in *C. elegans* were coincidental. To explore this, we delayed anaphase using a *such-1*^{ANAPC5}*(h1960)* mutant of the anaphase-promoting complex/cyclosome (APC/C)[32], labelling centrosomes and chromosomes using SPD-2^{CEP192}::GFP;HIS-58^{H2B}::mcherry. We tracked the centrosomes[16,19], observing oscillations before anaphase started (Table 1). The oscillations started when the posterior centrosome was at 70% of embryo length in both the control and the mutant, as we observed previously in *C. briggsae*[12]. In contrast, for both strains the die-down of oscillation occurred about two minutes after anaphase onset, regardless of the anaphase timing, thus leading to different durations (Table 1). We concluded that a positional switch controls anaphase oscillation onset in *C. elegans* embryos, while their ending point depends on the cell cycle. This "centrosome-tracking" assay was instrumental in our functional testing of the positional switch.

Microtubule contacts at the cortex depend upon centrosomal positioning.

To account for this positional switch, we hypothesized that the network of astral microtubules emanating from the posterior centrosome would have reduced accessibility to the "active region," the posterior crescent of the cortex where the active force generators are located[22]. When the spindle is close to the cell's centre, the density of microtubule contacts in the active region would be very low. This density would then increase as the posterior centrosome is displaced toward the posterior. The oscillations build up once a threshold of active force generators is reached, and they would depend on the position of the centrosome. We tested this by directly measuring the spatial distribution of the microtubule contacts at the cortex ("landing" assay). We were able to preserve the embryo shapes by using spinning disk microscopy and by measuring microtubule dynamics using α-tubulin rather than EB labelling (Supplementary Experimental Procedures). Because the dynamics are so fast, we viewed the cortical contacts at a speed of 10 frames per second. Our method generated an exponential distribution of residency times (Supplementary Fig. S1B) consistent with previously published values[25]. We calculated the distribution of the microtubule contacts along the AP axis. To reduce uncertainty, we block–averaged the distribution in ten equivalent regions along the AP axis, and used a 10-second running average. We observed spatial heterogeneity with high-density ridge lines and an overall increase in contacts between metaphase and anaphase, consistent with the increasing nucleation rate previously described[26] (Supplementary Fig. S1C). To test whether the ridge lines corresponded to the centrosomal position, we used a wide-field microscope to view the spindle plane in the same strain and at the same temperature. We tracked the centrosomes as we have previously described[19]. We then combined the results from both experiments and aligned them with anaphase onset (Supplementary Experimental Procedures). We found that centrosome positioning coincides with the ridge lines (Fig. 1). We had initially observed the positional switch on cortical pulling forces in one-cell *C. briggsae* embryos[12], apparently related to the modulation of microtubule cortical contacts. So we performed the same experiments in this species, obtaining similar results (Supplementary Fig. S2). We concluded that the distance of the centrosome to the

cortex strongly controls the number of microtubule end contacts in both species. As a consequence, the number of active region contacts increases with the posterior displacement of the spindle.

A comprehensive model for pulling force regulation and spindle oscillations

We expected that the modulation of microtubule contact density by the centrosome-to-cortex distance would regulate the cortical pulling forces and create the previously observed positional switch. Indeed, we have already reported on *C. briggsae* whose oscillations start 30 s after anaphase onset because of a delay in centrosome posterior displacement[12]. Here we observed (Table 1) that when the posterior centrosome is not far enough to the posterior, there are fewer microtubules at the cortex and not enough active force generators[19], thus preventing anaphase oscillation. Such a putative positional control of oscillation onset may seem to conflict with the initial tug-of-war hypothesis, which posits that both the build-up and die-down timings are regulated by the processivity of force generators[19], possibly related to mitosis progression[23]. We therefore expanded the initial model to quantitatively capture how the microtubule network could create a positional switch on cortical pulling forces.

Expanding the model to account for microtubule dynamics

We modelled the dynamic instability of microtubules, taking into account their alternating growth and shrinkage phases[33], but assuming that the force-dependence of the catastrophe rate is negligible[34]. We also assumed that catastrophes happen only at the cortex (no free end catastrophes), and that microtubules fully depolymerize upon shrinking (negligible rescue rates)[25,26,35] (Supplementary Text 2.1.1). We set a constant number of microtubule nucleation sites at the centrosomes, which were never empty[34], and the microtubules emanated from there in an isotropic angular distribution[26,36]. We computed the number of microtubules that reached the cortex in the active region (Fig. 2C, *left*, purple colour) as a function of the position of the posterior centrosome (Fig. 2A, black curve). This highlighted a steeper increase that starts at a point consistent with the onset of oscillation at 70% of embryo length. We modelled the embryo as an ellipsoid, but our result was independent of that hypothesis, as various superellipse based shapes[37] all yielded the same switch behaviour (Supplementary Fig. S3 and Text 2.1.3). We therefore continued modelling with an ellipsoid embryo shape. We concluded that microtubule dynamics can implement the experimentally observed positional switch by regulating the number of microtubules available to force generators. Furthermore, the large number of microtubules that reach the active region during mid and late anaphase is consistent with the previous tug-of-war model's assumption that microtubules saturate a limited number of cortical force generators during this period[19,38].

Accounting for force generator dynamics

Force generator dynamics set oscillation frequencies and determine peak amplitude and die-down timings[19]. To combine this regulation with the proposed control by microtubule dynamics, we modelled the binding of microtubules and force generators[9] as a first-order chemical reaction using the law of mass action, assuming no cooperative binding between force generators[39]. We estimated the association constant from the binding and unbinding rates used in the anaphase oscillation model (Supplementary Text 2.2.2)[19]. For the sake of clarity, we initially assumed a time-independent association constant for modelling the oscillation onset. This enabled us to compute the number of engaged force generators versus the posterior centrosome positions (Supplementary Text 2.2). We found that when the centrosome was far from the posterior tip, a scarcity of astral microtubule contacts in the active region of the cortex limited the number of engaged force generators to below the previously described oscillation threshold[19] (Fig. 2B, black line, and 2C, *left*). Upon posterior displacement of the centrosome past 60% of the AP axis, we observed a steep increase in engaged force generators, similar to the number of microtubule contacts (compare the black curves in Figure 2A and B). This was followed by a saturation starting from 70% of the AP axis. This switch-like behaviour is consistent with our positional switch hypothesis. The precise position at which oscillations started was dependent on the position of the active region boundary (Fig. 2B). We assumed that this region was set up by LET-99 force generator inhibition[22] and extended from 70 to 100% of the AP-axis[21] (see the experimental validation below). Thus, the positional switch is located at about 70% of the AP axis, consistent with our previous experiments, so we retained this position for the modelling and simulations which followed. The saturation of engaged force generators that we saw suggests that, during anaphase, the control parameter is their dynamics, not their quantity. This is coherent since oscillation peak and die-down timings are mostly independent of centrosome positioning but do occur after an anaphase onset delay (Table 1), as suggested by the initial model. In writing the law of mass action for the force generators, we assumed that the cell membrane cortical force

generator anchors diffuse fast enough to not be limiting (Supplementary Text 2.2.4). We checked this assumption by computing the number of engaged force generators versus the position of the posterior centrosome. This was done under microtubule-force generator binding modelled by applying the law of mass action to areal concentrations, and we again found a positional switch (compare Supplementary Fig. S4A and B, black lines). In conclusion, our model suggests that oscillation onset is specifically regulated by the posterior displacement of the posterior centrosome via the dynamics of astral microtubules.

Microtubule and force generator dynamics set two independent switches

We next wondered how processivity of the force generators (reflecting mitosis progression[19,23]) and the posterior centrosome's position combine to initiate oscillation. We completed our expanded model by making the microtubule-force generator association constant dependent on time through the off-rate, which is the inverse of processivity. The off-rate was the control parameter in the initial model, and it decreases along the course of mitosis[19] (Supplementary Text 2.2.5). In contrast, in the new model the force generator on-rate is not constant, depending both on the number of microtubules available at the cortex for binding a force generator (Supplementary Text 2.2.2), and on polarity[13] (Supplementary Text 3). This suggests that to enable oscillation, the posterior centrosome needs to be close to the posterior tip of the embryo, which supports our positional switch experiment (Fig. 2D, blue curve). In addition to a positional control, the processivity needs to be in a given range (Fig. 2D, blue region): out of this zone, the oscillations are dampened (Fig. 2D, white areas). This is consistent with control via a steady increase in processivity[19], and leads to a dual control of the pulling forces. Interestingly, as seen experimentally (Supplementary Text 2.2.5), the posterior centrosome position more strongly influences oscillation onset than die-down (Fig. 2D, green and blue curves). To summarize, we expanded our initial tug-of-war model by adding a positional switch to control oscillation onset and thus the pulling forces that contribute to spindle elongation and posterior displacement.

We then decided to validate the model using three experiments. We first tested whether the boundary of the active region sets the centrosome position that corresponds to oscillation onset. We then confirmed that the onset is not controlled by force generator activity (Supplementary Text 2.2.3). And finally, we tested the positional switch prediction which said that it is the position rather than the timing of oscillation onset that weakly depends on embryo length.

The position of the active region boundary controls oscillation onset

In building the model, we reported that the position where oscillation starts is controlled by the boundary of the region where the active force generators are confined. Our model predicted that when this active region extends more anteriorly, the oscillation start position is also displaced anteriorly (Fig. 2B, blue and green curves). To check this, we increased the active region by partially depleting the protein LET-99 by RNAi, which is thought to restrict the force generator regulators GPR-1/2 to that area[11]. In treated embryos, the active force generators are thought to extend across the embryo's entire posterior half[22]. Indeed, we observed that as compared to the control, the position at which oscillations began was significantly displaced towards the anterior (Fig. 3A), in agreement with the model's predictions. Interestingly, the oscillations also started earlier with respect to anaphase onset, further supporting the idea that the oscillation onset is independent of mitosis progression (Fig. 3B). We concluded that the position of the active region boundary probably controls the position where oscillation onset will occur.

Because the positional switch relies on microtubule dynamics, our expanded model predicts that the position of oscillation onset will be independent of the total number of force generators (Supplementary Fig. S6A) when this count is above the threshold required for oscillations. We previously produced data that suggested such a result[12], and these experiments are reproducible (Supplementary Text 2.2.3).

The oscillation onset position is less sensitive to embryo size

Our expanded tug-of-war model suggested that the oscillation onset position only weakly depends upon the length of the embryo (Fig. 4A). To investigate this increased robustness as compared to the initial model, we depleted C27D9.1 and CID-1 by RNAi to respectively obtain longer and shorter embryos. In both cases, the embryos were viable and showed no other visible phenotypes. We measured the variations in the timing and positioning of oscillation onset with respect to the variations in embryo length. For both cases, we fitted a linear model, measuring oscillation onset timing slopes 10 times larger than that of the

oscillation onset position (Fig. 4B-C). This further suggests that the positioning and timing of oscillation initiation are not correlated to anaphase onset. This is also perfectly consistent with the model's prediction that oscillation onset positions are less sensitive to embryo lengths (Fig. 4A). In contrast, embryo length does impact the point at which oscillation die-down begins (Fig. 4D), which is not a surprise since it is temporally controlled. We therefore concluded that these experiments validated the expanded tug-of-war model.

Sensitivity analysis of the oscillation onset positions using the new model

Using our expanded model, we performed a thorough sensitivity analysis (Supplementary Fig. S5). As expected, the microtubule counts (Supplementary Fig. S5F) and dynamics (Supplementary Fig. S5C) were critical for setting the position of oscillation onset. The embryo widths (Supplementary Fig. S5D) and proportional scaling (Supplementary Fig. S5E) were also influential, although to a lesser extent. Interestingly, as suggested by the robustness of the position of oscillation onset versus the embryo length (Fig. 4A), when the area is constant, the eccentricity has a reduced impact (Supplementary Fig. S5B). Similarly, the quantity (Supplementary Fig. S6A) and dynamics (Supplementary Fig. S4A) of the force generators appear to have only a small effect when they reach the oscillation threshold, as previously reported[19]. The cortical distribution of the force generators and their restriction to the active region are also key (Fig. 2B). In conclusion, the positional control of oscillation onset relies on microtubule dynamics, while mitosis progression control is performed through force generator processivity.

Astral microtubule dynamics regulate the final spindle position

Microtubule dynamics create feedback on the cortical pulling forces which set the spindle's final position.

Cortical pulling forces cause anaphase spindle oscillations, along with the posterior displacement of the spindle during late metaphase and anaphase[18,19]. In our initial model, we suggested that the final posterior centrosome position results from a balance between the cortical pulling forces and centring forces, which were modelled by a spring[19]. In contrast, in the improved model, the average number of engaged force generators depends not only on their dynamics but also on microtubule availability at the cortex, and thus centrosome positioning. We figured that the positional control of the pulling force generators causes a feedback loop on the final position of the spindle, which these forces contribute to setting. To investigate this hypothesis, we simulated posterior displacement using our expanded model with the TR-BDF2 algorithm[40] (Supplementary Text 3.1). To ensure the proper force balance on the spindle, we also included the anterior centrosome in the model by using a 0 to 40% active region corresponding to the area lacking LET-99[21]. However, we restricted the anterior centrosome to a fixed position. Furthermore, since the model is linearized it is limited to considering modest variations in parameters around their nominal values. On the anterior side, we used a two-fold lower force generator on-rate[13], which results in half the number of active force generators as found at the posterior[17]. We assumed that force applied to posterior centrosome and originated in anterior side is halved after anaphase onset because sister-chromatids separated. Finally, we modelled the centring force with a spring (according to [16]), using processivity to control the progression of mitosis[19]. We could reproduce the global kinematics of posterior displacement[16]: slow prior to anaphase, then accelerating afterward (Fig. 5, black curve, and Supplementary Fig. S7A5). In particular, the model accounts well for the final position of the posterior centrosome. On this basis, we aimed to test the model incorporating microtubule dynamics to explore the consequences of this inclusion on final spindle positioning.

The active region but not the total force generator count determines the final position of the spindle.

Consistent with observations in *let-99(RNAi)*-treated embryos (Fig. 3A),[22] the final position of the posterior centrosome was displaced anteriorly when the boundary of the posterior active crescent moved anteriorly, so long as the region was large enough to initiate posterior displacement in the first place (Supplementary Fig. S7B). This result differs from the initial model's prediction that under similar cortical forces, the posterior displacement would be the same[22]. The asymmetry in cortical pulling forces that cause the posterior displacement is due to a larger number of active force generators on the posterior side[17]. This was initially assumed to reflect an asymmetric total number of generators, and was recently proposed to be due to an asymmetric distribution of GPR-1/2, leading to an asymmetric binding rate of force generators to microtubules (on-rate)[13]. The initial model predicted a linear dependence between the number of active force generators and the final spindle position[16]. Our expanded model is less sensitive to

that count (Supplementary Fig. S7CD and Supplementary Text 2.2.3), which is consistent with the observed robustness of oscillation onset positioning (Supplementary Fig. S6C). This robustness is attributed to a smaller increase in cortical pulling forces when the centrosome moves further to the posterior after crossing the boundary position (Supplementary Fig. S7A4). In conclusion, the final spindle position's dependence on the cortical boundary rather than the number of active force generators present suggests that the initial tug-of-war model is not enough to correctly understand the mechanism of spindle final position determination, and that the microtubule dynamics also have to be considered.

The final spindle position is resistant to changes in the final force generator processivity.

In the initial model, the final spindle position was predicted to not only depend on the imbalance of force generator quantities or their on-rates, but also on their final processivity. This prediction does not reflect *such-1* mutant results. This mutation results in altered mitosis progression and thus probably altered final processivity but normal final posterior centrosomal positioning (Table 1)[23]. In contrast and in cases of moderate final processivity variations, our expanded model can account for this robustness (Fig. 5). The new model better explains the final spindle position's resilience in the face of changes in force generator quantities or dynamics, and this is particularly important since it is essential to the proper positioning of the cleavage furrow.

Discussion

In measuring the spatial distribution of microtubule contacts at the cell cortex, we found that it is uneven in space, concentrating more in the regions closer to the centrosomes. It is however noteworthy that due to the increased nucleation and persistence of microtubules, the total number of contacts scales up (Fig. 1, 80 s after anaphase onset), as expected from their regulation along the course of mitosis[26]. This contact distribution regulates the forces responsible not only for the anaphase spindle oscillations, but also for the spindle's posterior displacement. Interestingly, these causative forces are controlled by the positioning of the posterior centrosome, the so-called *positional switch*. The forces also contribute to spindle elongation, and their positional regulation might be linked to tension-based spindle assembly checkpoint satisfaction[41]. We expanded our tug-of-war spindle oscillation and posterior displacement model[19] to account for this, and validated it experimentally. In particular, we observed that the position of oscillation onset, but not the timing, is resistant to variations in embryo length. It is also correlated to the size of the posterior active force generator region, assumed to be limited by LET-99[21,22]. In the early stages of mitosis, the spindle lies in the middle of the embryo, and both of the centrosomes are far from their respective cortex. Therefore, the imbalance in active force generator quantities[17] causes a slight posterior pulling force, resulting in a slow posterior displacement[18] (Fig. 2C, *left*). The closer the posterior centrosome gets to the cortex, the larger the force imbalance becomes. This is because more microtubules reach the cortex, thus the pulling force builds up more rapidly, accelerating the posterior displacement. The number of engaged force generators increases, exceeding the threshold for oscillation onset[19] (Fig. 2C, *middle*). The pulling forces displacing the spindle start saturating, both because of the limited cortical anchors[19,42] and because once the posterior centrosome crosses the boundary of the active region, only the forces projected along the anteroposterior axis contribute to the spindle displacement (Supplementary Fig. S2C, *right*). Because they are opposing, these and the centring forces balance[19], setting the spindle's position at the end of mitosis.

This positional switch adds to the previously described temporal control by force generator processivity[19], which in turn reflects mitosis progression[23]. These two controls act independently, as they relate to two independent components: the *positional control* is determined by microtubule dynamics; and the *temporal control* is set by the force generator dynamics. Indeed, the curve reflecting the engaged force generator count versus the centrosome positioning (Fig. 2B) steeply increases starting at 60% of embryo length because of microtubule dynamics, while force generator dynamics cause the count to saturate above 70%. Our model suggests that there are two conditions necessary for oscillation onset (Fig. 2D, blue curve): enough microtubules in contact with the cortex's active region; and a force generator processivity that is high enough. Indeed, during anaphase, the temporal evolution of the cortical pulling force amplitudes is controlled by the force generator dynamics, as proposed previously and as indicated by the oscillation die-down timing[19]. This dual control of pulling forces was further confirmed by three experiments. First, we tested embryos treated with *let-99(RNAi)*. Their positional control is disturbed by anterior displacement of the active region boundary, and as predicted by the model (Supplementary Fig. S7B), the final centrosomal

position is strongly altered (Fig. 3A) although the oscillation die-down timing is not significantly different than for the control (Fig. 3B). A second experiment was done in *such-1(h1960)* mutants, where temporal control is altered by a delay in anaphase onset. In this case, the time between anaphase onset and oscillation die-down was the same as in the control, implying that they were delayed in the same proportion. In contrast, the oscillation onset and die-down positions were not altered by a delayed anaphase onset (Table 1). Finally, when we used a *gpr-2* mutant to decrease the number of active force generators, we observed a precocious oscillation die-down (Supplementary Fig. S6B). The force generator quantity exceeded the threshold during a shorter time period, consistent with the initial model's prediction (see e.g. Figure 5C in [19]). Overall, these experiments support the conclusion that force generator dynamics dominate the control of anaphase oscillations after their onset.

We hypothesized that these combined controls, in particular the proposed positional switch, confer some robustness to the final position of the posterior centrosome and consequently of the spindle. This may be due to buffering against variations in the initial centrosomal positions (Supplementary Fig. S7E), or may be caused by the final processivity, which determines the final cortical pulling forces (Fig. 5). In terms of asymmetric cell division, the final spindle position contributes to fixing the cytokinesis cleavage furrow position, essential for the correct distribution of cell polarity cues and thus daughter cell fates[1,2,5]. In addition to studying the *C. elegans* nematode alone, we also recently performed a comparative study between two nematode cousins (*C. elegans* and *C. briggsae*)[12]. We found that cortical force generator regulation is altered because there is a duplication in *C. elegans* (GPR-1 and GPR-2) while *C. briggsae* only displays GPR-2[12]. We proposed that this evolution was made possible by the positional switch and the resulting resistance to force generator quantity and dynamics. Indeed, *C. briggsae* microtubule contacts at the cell cortex are distributed as they are in *C. elegans* (Supplementary Fig. S3), and resistance to embryo length variations is also observed[12]. Interestingly, the positional control of anaphase oscillation onset in *C. briggsae* results in a 30 s delay between oscillation and anaphase onsets (attributed to spindle "overcentration"[12]), while the oscillation die-down is synchronous with anaphase onset as predicted by our model. Furthermore, cross-species insertion of GPR genes modulates oscillation amplitude but preserves the positional switch, which is consistent with our *gpr-2(ok1179)* experiment. The robustness of final spindle positioning is likely to be true in more than just these two species[43]. During the course of evolution, the proposed robustness mechanism has enabled changes in the regulation of nuclei/centrosome complex position, even though the regulation is essential.

The dynamic instability of microtubules is at the core of this robustness mechanism. More precisely, it relies on the number of microtubule cortical contacts, which reflects the distance between the centrosome and the cortex. Indeed, said distance is measured in "units of microtubule dynamics" (Supplementary Text 2.1.2). This is a classic mechanism for creating centring[28,44] or other shape-dependent mechanisms[29,45,46], although it was always inferred from cell-level properties. In contrast, the distribution of the microtubule end contacts located at the cortex was obtained from microscopic measurements. We observed a density ratio of about 2 between the regions with the most and least microtubule contacts at a given time, and this ratio represents the sensitivity to centrosomal position (Supplementary Text 2.1.2). From a theoretical point of view, considering the ellipsoidal shape of the *C. elegans* embryo and the microtubule dynamics measurements (see above), the predicted maximal ratio is 1.64. Our experimental result is close to this prediction, suggesting that the microtubule dynamics parameters are optimal for the positional control we discuss here.

Conclusion

The study of the mechanism leading to the precise timing and positioning of the transverse oscillation onset in the *C. elegans* embryo has highlighted the key role of microtubule dynamics in probing the boundary of the active force generator region. This *positional control* of spindle rocking acts in addition to previously described regulation via pulling force machinery dynamics (*temporal control*). Both controls set independent switches to prevent premature force bursts. The finding of this supplementary positional control paves the way to understanding a novel mitosis choreography mechanism, going further than regulation by just the cell cycle.

At anaphase, the positional control we report on here prevents the application of strong forces to the spindle before it reaches the point at which it normally elongates. We suggest that this control contributes to ensuring the correct positioning of cytokinesis cleavage furrow assembly. Indeed, this is positioned by two independent signals[47]. The first is the central spindle at the position where the spindle reaches its full elongation[48]. This elongation in turn requires cortical pulling forces[10], the regulation of which we investigated here. Therefore, the positional control of anaphase force bursts guarantees that the central spindle-signalling of the cleavage furrow will occur in the correct position.

At telophase, the cleavage furrow position is signalled by the spindle poles[49]. Interestingly, our proposed positional switch controls the final centrosome positions, since the forces that displace them are due to the same generators as spindle rocking and elongation. The mechanism ensures that the posterior centrosome has a robust final position that is scaled with the AP axis. Overall, the positional switch confers robustness to both signals that set the cleavage furrow position, therefore guaranteeing proper polarity cue distribution and the correct daughter cell fates[6,7]. We previously proposed that such a mechanism buffered changes in cortical pulling force levels and timings between the *C. elegans* and *C. briggsae* nematodes. This permitted substantial modifications in the essential GPR-1/2^{LGN} genes, which are part of the complex that generates cortical pulling forces[12].

Finally, the observed positional switch is caused by astral microtubules. They provide feedback about the posterior centrosome position to the cortical pulling forces which cause spindle displacement and rocking. This finding is a novel example of a microfilament-based system that controls essential aspects of cell division, such as cleavage furrow positioning and the granting of resistance to perturbation. In contrast with robustness resulting from classic biochemical signalling pathways[50,51], this mechanism is based solely on cell mechanics and component dynamics.

Material and Methods

Culturing C. elegans

C. elegans nematodes were cultured as described in [52], and dissected to obtain embryos. The strains were maintained at 25°C and imaged at 23°C, with the exception of the *gpr-2* mutant, *such-1* mutant, and their controls, which were maintained at 15°C and imaged at 18°C. The strains were handled on nematode medium plates and fed with OP50 bacteria.

Strains

TH65 *C. elegans* (*Ce*) YFP::TBA-2 (α-tubulin)[26] and ANA020 *C. briggsae* (*Cb*) GFP::β-tubulin strains with a microtubule fluorescent labelling were used as the controls for the "landing" assay. TH27 *C. elegans* GFP::TBG-1 (γ-tubulin)[53] and *C. briggsae* ANA022 TBG-1::GFP strains[12] displaying a centrosomal fluorescent labelling were the standards for the "centrosome-tracking" assay. For event timing, the control was the *C. elegans* TH231 (SPD-2::GFP) strain with centrosome labelling crossed to OD56 (mCherry::HIS-58) histone labelling (Table 1). It was crossed with the KR4012 *such-1(h1960)* mutant strain[32] to create JEP16. Centrosome tracking upon mutating *gpr-2* was performed on the JEP14 strain, which was obtained by crossing the 10x backcrossed strain TH291 *gpr-2*(*ok1179*) and TH27 *C. elegans* GFP::TBG-1 (γ -tubulin).

Gene inactivation through mutants or protein depletion by RNAi feeding

RNAi experiments were performed by ingestion of transformed HT115 bacteria. *let-99*, *cid-1* and *c27d9.1* genes were amplified from AF16 genomic ADN and cloned into the L4440 plasmid. To obtain stronger phenotypes, the feeding was performed at 20°C for 48h (except for *let-99*, which was only done for 16-24h). The control embryos for the RNAi experiments were treated with bacteria carrying the empty plasmid L4440.

Preparation of the embryos for imaging

Embryos were dissected in M9 buffer and mounted on a pad (2% w/v agarose, 0.6% w/v NaCl, 4% w/v sucrose) between a slide and a coverslip. Depending on the assay, they were observed using different microscopic setups. To confirm the absence of phototoxicity and photodamage, we checked for normal rates of subsequent divisions[54]. Fluorescent lines were imaged at 23°C unless otherwise indicated.

Imaging of microtubule contacts at the cortex ("landing" assay)

We imaged *C. elegans* or *C. briggsae* one-cell embryos at the cortex plane in contact with the glass slide (Supplementary Fig. S1A), viewing from the nuclear envelope breakdown (NEBD) until the end of cell division. We did our utmost to preserve the embryo shapes. The thickness of the perivitelline space[55] therefore meant we had to use spinning disk microscopy rather than TIRF (Supplementary Fig. S1A). Cortical microtubule contact tracking was thus performed on a LEICA DMI6000 / Yokogawa CSU-X1 M1 spinning disc microscope, using a HCX Plan Apo 100x/1.4 NA oil objective. Illumination was performed using a white-light Fianium laser filtered around 514 nm in a homemade setup. To account for the fast speed of microtubule dynamics at the cortex, images were acquired at an exposure time of 100 ms (10 Hz) using an ultra-sensitive Roper Evolve EMCCD camera and the MetaMorph software (Molecular Devices) without binning. During the experiments, the embryos were kept at 23°C. To image embryos at the cortex, we typically moved the focus to 12 to 15 µm below the spindle plane (Supplementary Fig. S1A).

Centrosome imaging

For the "centrosome-tracking" and the "event-timing" assays, embryos were observed at the midplane using a Zeiss Axio Imager upright microscope modified for long-term time-lapse. First, an extra anti-heat filter was added to the mercury lamp light path. Secondly, to decrease the bleaching and obtain optimal excitation, we used an enhanced transmission 12 nm band pass excitation filter centred on 485 nm (AHF analysentechnik). We used a 100x/1.45 NA Oil plan-Apo objective. Images were acquired with an Andor iXon3 EMCCD 512x512 camera at 33 frames per second and using their Solis software. The beginning of the spindle's abrupt elongation (Supplementary Fig. S8A) was used as the marker for anaphase onset[16], and the centrosome tracks of individual embryos were aligned with this for averaging purposes or for overlay on the "landing" assay.

Statistics

Averaged values were compared using the two-tailed Student's *t*-test with correction for unequal variance except where otherwise stated. For the sake of simplicity, we recorded confidence levels using stars (*, $p \leq 0.05$; **, $p \leq 0.005$; ***, $p \leq 0.0005$; ****, $p \leq 0.00005$) and n.s. (non-significant, $p > 0.05$; sometimes omitted to save room). We abbreviated standard deviation by SD, standard error by s.e., and standard error of the mean by s.e.m.

Data processing, modelling, and simulation

All data analysis was developed using Matlab (The MathWorks). Modelling was performed using Wolfram Mathematica formal calculus software. Numerical simulations were performed using Matlab and Simulink (The MathWorks).

References

1. Betschinger J, Knoblich JA. Dare to be different: asymmetric cell division in Drosophila, C. elegans and vertebrates. *Curr Biol* **14**, R674-685 (2004).

2. Gillies TE, Cabernard C. Cell division orientation in animals. *Curr Biol* **21**, R599-609 (2011).

3. Rappaport R. Cytokinesis in animal cells. *Int Rev Cytol* **31**, 169-213 (1971).

4. Knoblich JA. Asymmetric cell division: recent developments and their implications for tumour biology. *Nat Rev Mol Cell Biol* **11**, 849-860 (2010).

5. White EA, Glotzer M. Centralspindlin: At the heart of cytokinesis. *Cytoskeleton (Hoboken)* **69**, 882-892 (2012).

6. Morin X, Bellaiche Y. Mitotic spindle orientation in asymmetric and symmetric cell divisions during animal development. *Dev Cell* **21**, 102-119 (2011).

7. Gonczy P. Mechanisms of asymmetric cell division: flies and worms pave the way. *Nat Rev Mol Cell Biol* **9**, 355-366 (2008).

8. McNally FJ. Mechanisms of spindle positioning. *J Cell Biol* **200**, 131-140 (2013).

9. Nguyen-Ngoc T, Afshar, K., and Gonczy, P. Coupling of cortical dynein and G alpha proteins mediates spindle positioning in Caenorhabditis elegans. Nat. Cell Biol. *9* **1294-1302**, (2007).

10. Colombo K, Grill SW, Kimple RJ, Willard FS, Siderovski DP, Gonczy P. Translation of polarity cues into asymmetric spindle positioning in Caenorhabditis elegans embryos. *Science* **300**, 1957-1961 (2003).

11. Park DH, Rose LS. Dynamic localization of LIN-5 and GPR-1/2 to cortical force generation domains during spindle positioning. *Dev Biol* **315**, 42-54 (2008).

12. Riche S, Zouak M, Argoul F, Arneodo A, Pecreaux J, Delattre M. Evolutionary comparisons reveal a positional switch for spindle pole oscillations in Caenorhabditis embryos. *J Cell Biol* **201**, 653-662 (2013).

13. Rodriguez Garcia R, Chesneau L, Pastezeur S, Roul J, Tramier M, Pecreaux J. Dynamics of dynein at microtubule plus-ends and the cortex during the division of the C. elegans zygote. *bioRxiv preprint*, 118604 (2017).

14. Ahringer J. Control of cell polarity and mitotic spindle positioning in animal cells. *Curr Opin Cell Biol* **15**, 73-81 (2003).

15. Kimura A, Onami S. Local cortical pulling-force repression switches centrosomal centration and posterior displacement in C. elegans. *J Cell Biol* **179**, 1347-1354 (2007).

16. Pecreaux J, *et al.* The Mitotic Spindle in the One-Cell C. elegans Embryo Is Positioned with High Precision and Stability. *Biophys J* **111**, 1773-1784 (2016).

17. Grill SW, Howard J, Schaffer E, Stelzer EH, Hyman AA. The distribution of active force generators controls mitotic spindle position. *Science* **301**, 518-521 (2003).

18. Labbe JC, McCarthy EK, Goldstein B. The forces that position a mitotic spindle asymmetrically are tethered until after the time of spindle assembly. *J Cell Biol* **167**, 245-256 (2004).

19. Pecreaux J, *et al.* Spindle oscillations during asymmetric cell division require a threshold number of active cortical force generators. *Curr Biol* **16**, 2111-2122 (2006).

20. Grill SW, Gonczy P, Stelzer EH, Hyman AA. Polarity controls forces governing asymmetric spindle positioning in the Caenorhabditis elegans embryo. *Nature* **409**, 630-633 (2001).

21. Wu JC, Rose LS. PAR-3 and PAR-1 inhibit LET-99 localization to generate a cortical band important for spindle positioning in Caenorhabditis elegans embryos. *Mol Biol Cell* **18**, 4470-4482 (2007).

22. Krueger LE, Wu JC, Tsou MF, Rose LS. LET-99 inhibits lateral posterior pulling forces during asymmetric spindle elongation in C. elegans embryos. *J Cell Biol* **189**, 481-495 (2010).

23. McCarthy Campbell EK, Werts AD, Goldstein B. A cell cycle timer for asymmetric spindle positioning. *PLoS Biol* **7**, e1000088 (2009).

24. Labbe JC, Maddox PS, Salmon ED, Goldstein B. PAR proteins regulate microtubule dynamics at the cell cortex in C. elegans. *Curr Biol* **13**, 707-714 (2003).

25. Kozlowski C, Srayko M, Nedelec F. Cortical microtubule contacts position the spindle in C. elegans embryos. *Cell* **129**, 499-510 (2007).

26. Srayko M, Kaya A, Stamford J, Hyman AA. Identification and characterization of factors required for microtubule growth and nucleation in the early C. elegans embryo. *Dev Cell* **9**, 223-236 (2005).

27. Dogterom M, Yurke B. Microtubule dynamics and the positioning of microtubule organizing centers. *Physical Review Letters* **81**, 485-488 (1998).

28. Dogterom M, Kerssemakers JW, Romet-Lemonne G, Janson ME. Force generation by dynamic microtubules. *Curr Opin Cell Biol* **17**, 67-74 (2005).

29. Minc N, Burgess D, Chang F. Influence of cell geometry on division-plane positioning. *Cell* **144**, 414-426 (2011).

30. Thery M, Jimenez-Dalmaroni A, Racine V, Bornens M, Julicher F. Experimental and theoretical study of mitotic spindle orientation. *Nature* **447**, 493-496 (2007).

31. Tsou MF, Ku W, Hayashi A, Rose LS. PAR-dependent and geometry-dependent mechanisms of spindle positioning. *J Cell Biol* **160**, 845-855 (2003).

32. Tarailo M, Kitagawa R, Rose AM. Suppressors of spindle checkpoint defect (such) mutants identify new mdf-1/MAD1 interactors in Caenorhabditis elegans. *Genetics* **175**, 1665-1679 (2007).

33. Mitchison T, Kirschner M. Dynamic instability of microtubule growth. *Nature* **312**, 237-242 (1984).

34. Howard J. Elastic and damping forces generated by confined arrays of dynamic microtubules. *Phys Biol* **3**, 54-66 (2006).

35. O'Rourke SM, Christensen SN, Bowerman B. Caenorhabditis elegans EFA-6 limits microtubule growth at the cell cortex. *Nat Cell Biol* **12**, 1235-1241 (2010).

36. O'Toole ET, McDonald KL, Mantler J, McIntosh JR, Hyman AA, Muller-Reichert T. Morphologically distinct microtubule ends in the mitotic centrosome of Caenorhabditis elegans. *J Cell Biol* **163**, 451-456 (2003).

37. Edwards J. *An elementary treatise on the differential calculus, with applications and numerous examples*. Macmillan (1892).

38. Grill SW, Kruse K, Julicher F. Theory of mitotic spindle oscillations. *Physical Review Letters* **94**, 108104 (2005).

39. Koonce MP, Tikhonenko I. Dynein Motor Mechanisms. In: *Dyneins : structure, biology and disease* (ed^(eds King SM). 1st edn. Academic Press (2012).

40. Hosea ME, Shampine LF. Analysis and implementation of TR-BDF2. *Applied Numerical Mathematics* **20**, 21-37 (1996).

41. Cimini D, Wan X, Hirel CB, Salmon ED. Aurora kinase promotes turnover of kinetochore microtubules to reduce chromosome segregation errors. *Curr Biol* **16**, 1711-1718 (2006).

42. Grill SW, Hyman AA. Spindle positioning by cortical pulling forces. *Dev Cell* **8**, 461-465 (2005).

43. Farhadifar R, *et al.* Scaling, selection, and evolutionary dynamics of the mitotic spindle. *Curr Biol* **25**, 732-740 (2015).

44. Wuhr M, Dumont S, Groen AC, Needleman DJ, Mitchison TJ. How does a millimeter-sized cell find its center? *Cell Cycle* **8**, 1115-1121 (2009).

45. Daga RR, Nurse P. Interphase microtubule bundles use global cell shape to guide spindle alignment in fission yeast. *J Cell Sci* **121**, 1973-1980 (2008).

46. Thery M. Micropatterning as a tool to decipher cell morphogenesis and functions. *J Cell Sci* **123**, 4201-4213 (2010).

47. Bringmann H, Hyman AA. A cytokinesis furrow is positioned by two consecutive signals. *Nature* **436**, 731-734 (2005).

48. Lewellyn L, Dumont J, Desai A, Oegema K. Analyzing the effects of delaying aster separation on furrow formation during cytokinesis in the Caenorhabditis elegans embryo. *Mol Biol Cell* **21**, 50-62 (2010).

49. Bringmann H, Cowan CR, Kong J, Hyman AA. LET-99, GOA-1/GPA-16, and GPR-1/2 are required for aster-positioned cytokinesis. *Curr Biol* **17**, 185-191 (2007).

50. McIntosh JR, Molodtsov MI, Ataullakhanov FI. Biophysics of mitosis. *Quarterly reviews of biophysics* **45**, 147-207 (2012).

51. Musacchio A. Spindle assembly checkpoint: the third decade. *Philos Trans R Soc Lond B Biol Sci* **366**, 3595-3604 (2011).

52. Brenner S. The genetics of Caenorhabditis elegans. *Genetics* **77**, 71-94 (1974).

53. Oegema K, Desai A, Rybina S, Kirkham M, Hyman AA. Functional analysis of kinetochore assembly in Caenorhabditis elegans. *The Journal of Cell Biology* **153**, 1209-1226 (2001).

54. Riddle DL. *C. elegans II*. Cold Spring Harbor Laboratory Press (1997).

55. Olson SK, Greenan G, Desai A, Muller-Reichert T, Oegema K. Hierarchical assembly of the eggshell and permeability barrier in C. elegans. *J Cell Biol* **198**, 731-748 (2012).

Acknowledgments

The 10 times backcrossed strain *gpr-2(ok1179)* was a kind gift from Prof. Anthony A. Hyman. We thank Dr Grégoire Michaux for the feeding clone library and technical support. We also thank Drs Benjamin Mercat, Anne Pacquelet, Xavier Pinson, Yann Le Cunff, Danielle Fairbrass, Grégoire Michaux, Roland Le Borgne, Sébastien Huet, Marc Tramier, Claude Prigent, Françoise Argoul, and Alain Arnéodo for technical help, critical comments on the manuscript, and discussions about the project. JP was supported by a CNRS ATIP starting grant and *La ligue nationale contre le cancer*. We also acknowledge *plan cancer* grant BIO2013-02, COST EU action BM1408 (GENiE) and *la ligue contre le cancer (comités d'Ille-et-Vilaine et du Maine-et-Loire)*. Some strains were provided by the CGC, which is funded by NIH Office of Research Infrastructure Programs (P40 OD010440; University of Minnesota, USA). Microscopy imaging was performed at the MRIC facility, UMS 3480 CNRS / US 18 INSERM / University of Rennes 1. Spinning disk microscope was co-funded by the CNRS, *Rennes Métropole* and *Region Bretagne* (AniDyn-MT grant). HB's postdoctoral fellowship was funded by *Region Bretagne* (AniDyn-MT grant) and the European Molecular Biology Organization.

Author contributions

Conceptualization, JP, HB, and MD; Methodology, HB, LC, and JP; Software, JP and HB; Validation / Formal Analysis, HB, SP, and LC; Investigations / Data Curation, HB, SP, LC, and JP; Writing – Original Draft, HB and JP; Writing - Review & Editing, HB, LC, MD, and JP; Supervision, JP.

Competing financial interests

No competing financial interests.

Figures

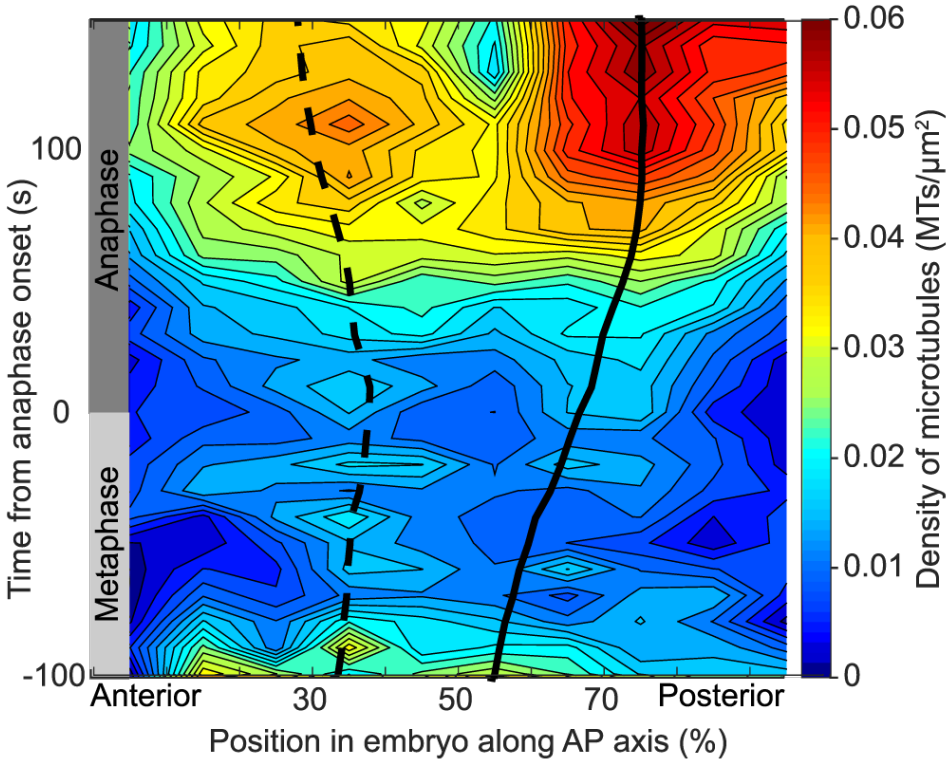

Figure 1: Microtubule contact density at the cell cortex in *Caenorhabditis elegans.* Microtubule contact density at the cortex obtained by spinning disk microscopy, and viewing a YFP::α-tubulin strain (see Methods). The densities were averaged along the AP axis (in 10 regions of equal width) and across time (10 s running window), shown here as a heat map (*N* = 22 *C. elegans* embryos). The trajectories of the centrosomes obtained by imaging the same strain in the spindle plane were superimposed (*N* = 8). The dashed line represents the anterior centrosome trajectory, and the solid line indicates the posterior one.

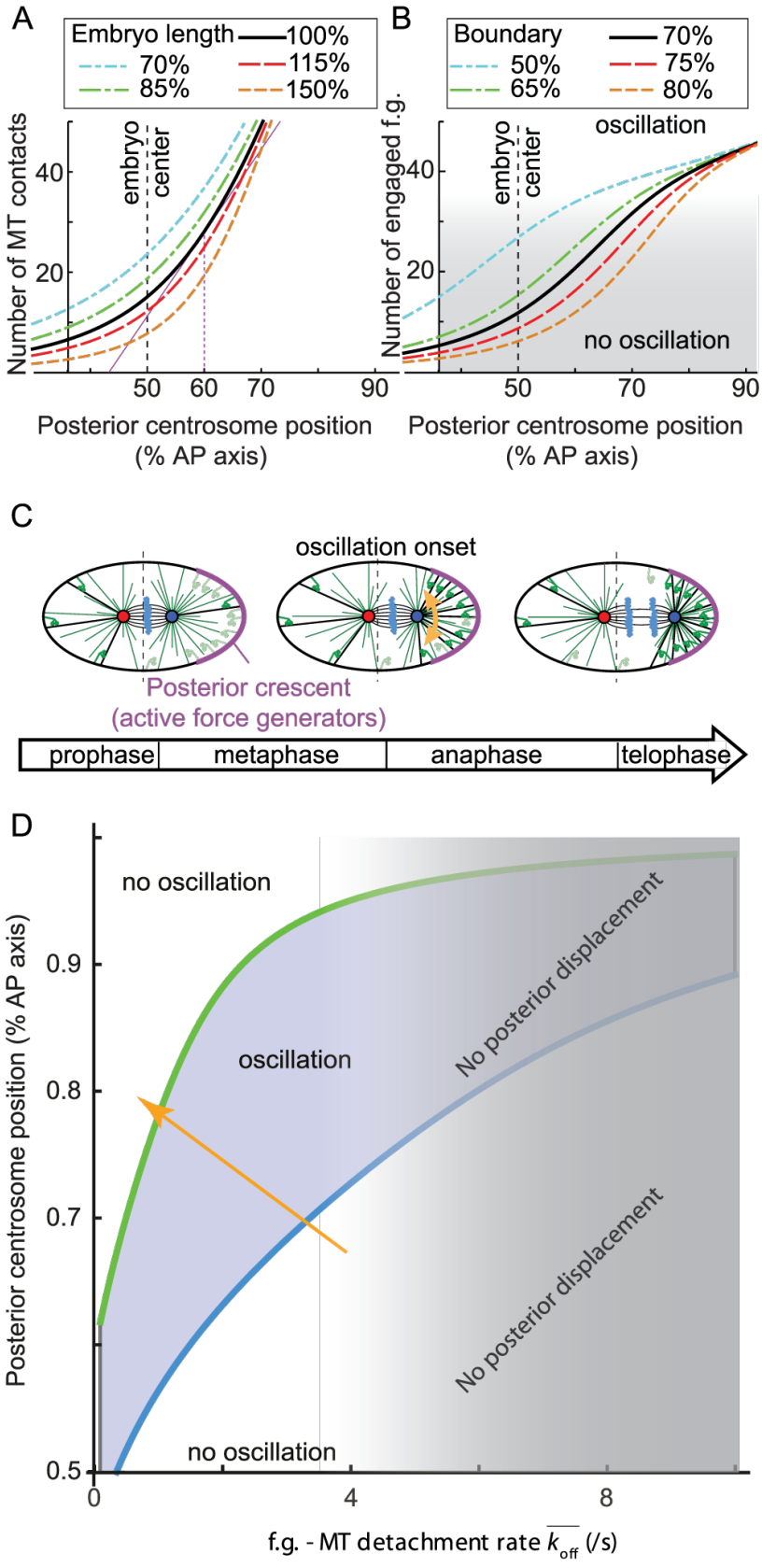

Figure 2: Expanded "tug-of-war" model of pulling force regulation and spindle oscillations. (**A**) Modelled number of microtubules (MTs) contacting the cortex in the active region having a boundary at 70% of the current anteroposterior (AP) axis versus the posterior displacement of the centrosome along that axis. The embryo length varies from 70

to 150% of the length of the untreated one (Supplementary Text 2.1.3). For the untreated embryo (thick black line), when the centrosome position was above 60%, the number of contacts started to increase steeply (purple line). (**B**) Number of engaged force generators versus the posterior displacement of the centrosome along the AP axis, with the active region boundary expressed as a percentage of embryo length (Supplementary Text 2.2.2). The thick black line represents a boundary at 70%, mimicking the untreated embryo. In this case, when the centrosome reached 60% of the AP axis, the number of engaged force generators increased steeply and saturated above 70%, causing a switch-like behavior. Blue and green curves show *let-99(RNAi)* experiments where the boundary was displaced anteriorly. Red and orange curves show cases of posteriorly displaced boundaries. Gray shading indicates when the number of engaged force generators was too low to permit oscillation (below threshold). (**C**) Expanded tug-of-war schematic representation. At early metaphase, the spindle is roughly centered (*left*); around anaphase onset, it reaches 70% of the AP axis and starts oscillating (*middle,* orange arrow); and after anaphase, it reaches its final position, about 80% of AP axis (*right*). The anterior and posterior centrosomes are red and blue disks, respectively, and the chromosomes are light blue clouds. Microtubules that emanate from the centrosomes will either reach the cortex and find an active force generator (thick black lines), or reach an inactive region of the cortex or be too short to reach the cortex (thin green lines). The posterior crescent containing the active force generators is purple, and inactive and engaged (i.e. active) force generators are light and dark green, respectively. Within the spindle, microtubules are represented by thin black lines. A vertical dashed line marks the middle of the AP axis. **(D)** Stability diagram of the expanded model as a function of the detachment rate (off-rate $\overline{k_{off}}$, inverse of the processivity, *x*-axis) and of the position of the centrosome as a percentage of embryo length (*y*-axis). The unstable region (blue) corresponds to the values of off-rate and posterior-centrosomal position enabling oscillation development (Supplementary Text 2.2.5). The critical values are marked by the thick blue and green lines. The orange arrow indicates the typical phase trajectory during mitosis based on the parameters used in this study. The greyed-out area shows that above a detachment rate threshold, the posterior displacement of the spindle/posterior centrosome no longer occurs (orange curve in Figure 5). The centrosome needs to reach a position that is posterior enough to enable oscillations while force generators display a realistic processivity (measured to 1-2 s^{-1} in metaphase[13]). Furthermore, the sloping blue line corresponding to oscillation onset suggests that it is controlled by both position and processivity. In contrast, the steep green return-to-stability line, showing the oscillation die-down, suggests that this phenomenon depends mostly on processivity. For all plots, the parameters used are listed in Supplementary Text 4.

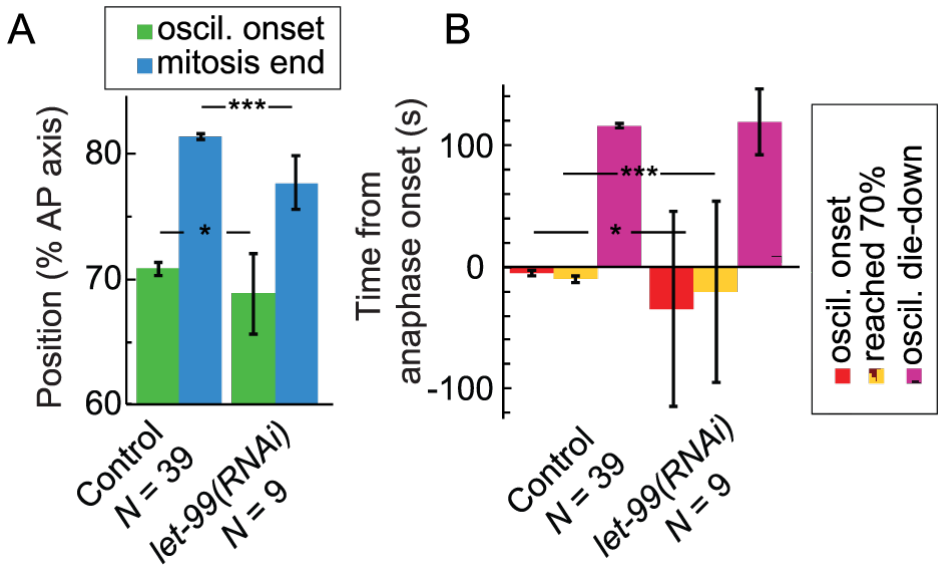

Figure 3: Force generator locations contribute to setting the positional switch on cortical pulling forces. (A) Positions of the posterior centrosome at oscillation onset and die-down. **(B)** Timings of oscillation onset, die-down, and their arrival at 70% of embryo length when the size of the active region is changed. We measured *let-99(RNAi)* (*N* = 9) and untreated (*N* = 39) embryos at 23ºC, with centrosomes labelled by GFP::γ-tubulin. Error bars indicate SD, and asterisks indicate significant differences (see Methods).

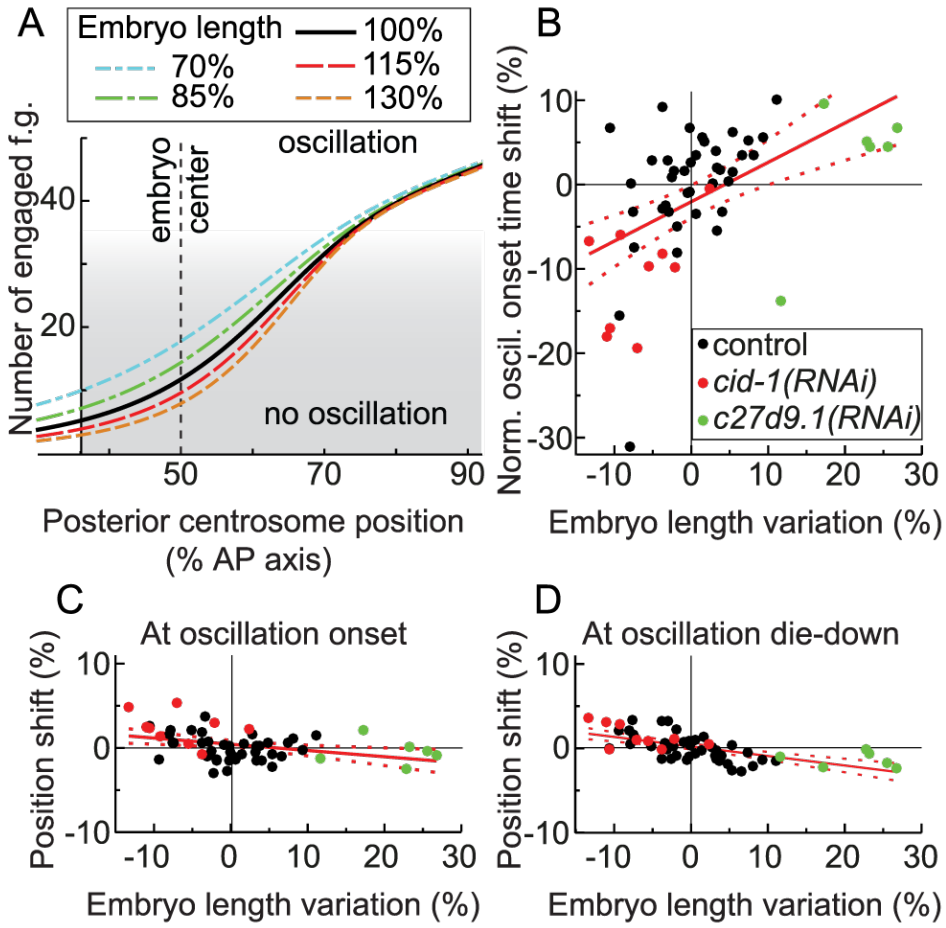

Figure 4: Embryo length has less effect on oscillation onset and die-down positions than on their timing. (A) Modelled number of microtubules contacting the active region of the cortex *versus* the posterior displacement of the centrosome along the AP axis as a percentage of embryo length. The line colours indicate the embryo length: untreated embryos are black; the shorter embryos produced by *cid-1(RNAi)* are blue and green; and the longer ones from *c27d9.1(RNAi)* are red and orange. The parameters used are listed in Supplementary Text 4. Grey shading indicates when the number of engaged force generators was too low to permit oscillation (below threshold). **(B-D)** Variations in embryo lengths as compared to the control (normalized by the average length, see Supplementary Experimental Procedures) are shown here versus the (B) shift in oscillation onset normalized by the control's average pro-metaphase and metaphase duration; and versus the (C) oscillation onset and (D) die-down positions as compared to the control. The solid red lines indicate the linear least square fits, with slopes of 0.47 ± 0.11 (p = 5 × 10^{-5} compared to null slope), -0.07 ± 0.02 (p = 0.005) and -0.11 ± 0.02 (p = 2.6 × 10^{-7}), respectively. The red dashed line is the standard error of the mean. We measured N = 9 *cid-1(RNAi)*, N = 6 *c27d9.1(RNAi),* and N = 39 untreated embryos with GFP::γ-tubulin-labelled centrosomes at 23ºC. The control embryos used are the same as shown in Figure 3. Dots indicate individual embryos, and the average control values (0 shift) are thin black lines.

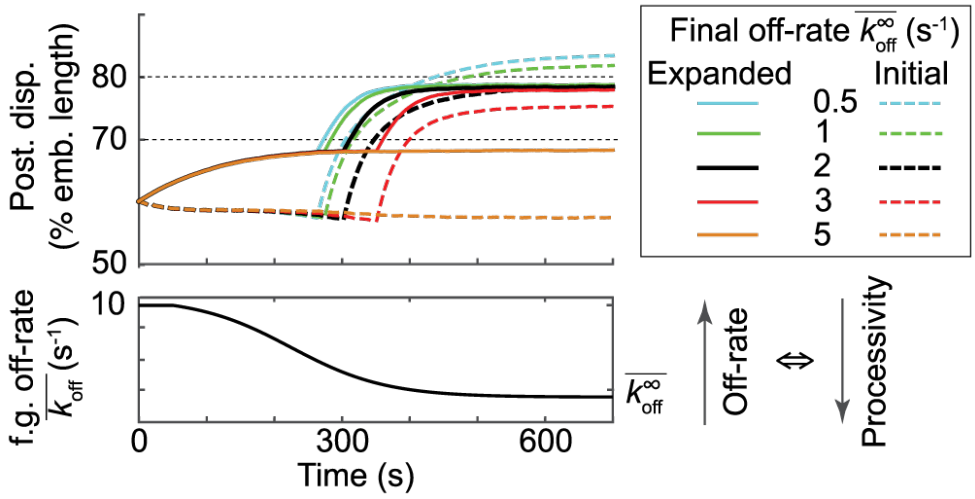

Figure 5: The expanded model of pulling force regulation offers resistance to final force generator processivity variations. Color-coded stochastic simulations of the displacement of the posterior centrosome when varying the final force generator (f.g.) detachment rate (off-rate, the inverse of the processivity). The dashed lines indicate the results from the initial model, and the solid lines are from the expanded one (Supplementary Text 3). A typical example of f.g. off-rate evolution throughout mitosis is shown at the bottom. Earlier than 300 s, whatever their final values are, detachment rates are very close, leading to superimposed posterior centrosome trajectories. The dispersion of the final values from the initial model revealed a lack of robustness to variations in the final off-rate that disappeared in the expanded model. The parameters used are listed in Supplementary Text 4.

Table

Characteristic measured (mean ± s.e.m.)	control (*N* = 17)	*such-1(h1960)* (*N* = 15)
Oscillation onset *T1* (s)	-11.03 ± 5.50	-39.83 ± 5.93 $p = 9 \times 10^{-4}$
Posterior centrosome (CS) reaching 70% of AP axis *T2* (s)	-11.76 ± 5.68	-85.50 ± 17.15 $p = 6 \times 10^{-4}$
From oscillation onset to post. CS reaching 70% *T1* - *T2* (s)	0.74 ± 4.96	45.67 ± 15.82 $p = 0.015$
Maximum oscillation amplitude (posterior) (%)	20.78 ± 0.65	22.71 ± 0.61 $p = 0.035$
Nuclear envelope breakdown time (s)	- 164.84 ± 3.48	- 291.04 ± 5.40 $p = 1 \times 10^{-17}$
Oscillation die-down *T3* (s)	124.4 ± 7.0	117.5 ± 7.63 $p = 0.507$
Oscillation duration *T3* - *T1* (s)	135.4 ± 8.9	157.3 ± 9.7 $p = 0.11$
Posterior centrosome position at oscillation onset (%)	70.68 ± 0.89	70.76 ± 0.49 $p = 0.936$
Posterior centrosome position at oscillation die-down (%)	79.51 ± 0.40	79.01 ± 0.69 $p = 0.515$
Embryo length (µm)	52.60 ± 0.86	53.98 ± 0.80 $p = 0.237$
Embryo width (µm)	35.21 ± 0.61	33.25 ± 0.53 $p = 0.019$

Table 1: Timing and position of metaphase and anaphase events in untreated embryos and in delayed-anaphase mutants. Embryos labelled with SPD-2^{CEP192}::GFP;HIS-58^{H2B}::mcherry were viewed at 18°C, and spindle poles tracked. We compared untreated embryos with an ANAPC5 homolog mutant, the *such-1(h1960)* whose gene codes for an APC/C[32]. Times were measured from the onset of anaphase, and the peak-to-peak oscillation amplitude is shown as a percentage of embryo width. Positions along the AP axis are shown as a percentage of embryo length. Error bars indicate the standard error of the mean. *p* values are reported for Student's *t*-test.

Supplementary Figures

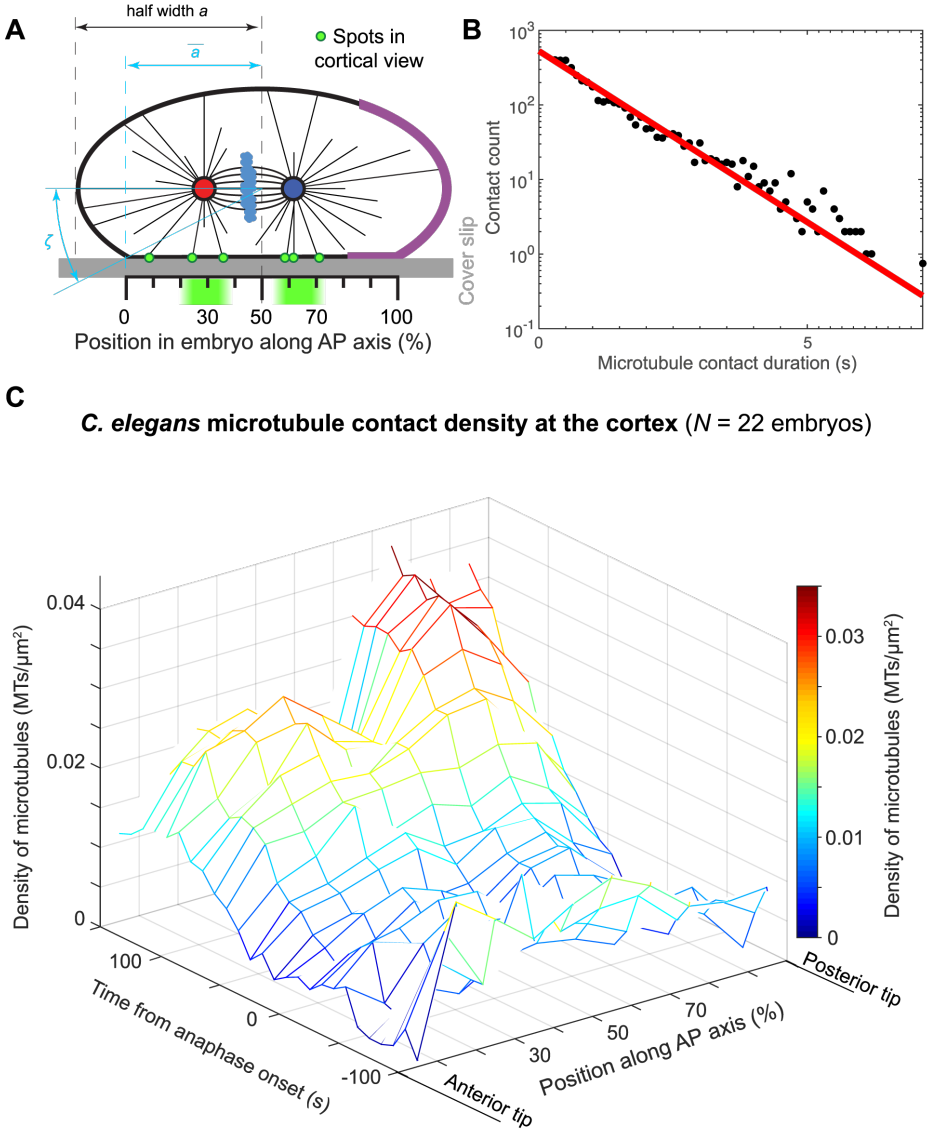

Figure S1: Density of microtubule contacts at the cell cortex in *C. elegans*.
(**A**) Experimental setup for viewing microtubule (MT) contact density at the cell cortex. The scale represents the 10 regions along the anteroposterior (AP) axis used for analysis (see Methods). Red and blue disks represent the anterior and posterior centrosomes, respectively, and the light blue clouds are the chromosomes. Microtubules emanating from the centrosomes are thin black lines. The posterior crescent where the active force generators are located is the purple cortical region. (**B**) semi-log histogram of the residency times (in second) during metaphase and anaphase for a single embryo (black dots), fitted with an exponential (red line) 0.95 ± 0.03 s decay time (N = 3832 MTs). (**C**) MT contact density at the cortex obtained by analysing spinning disk microscopy images of the YFP::α-tubulin-labelled microtubule strain (see Methods) (N = 22 *C. elegans* embryos). The data are the same as in Fig. 1.

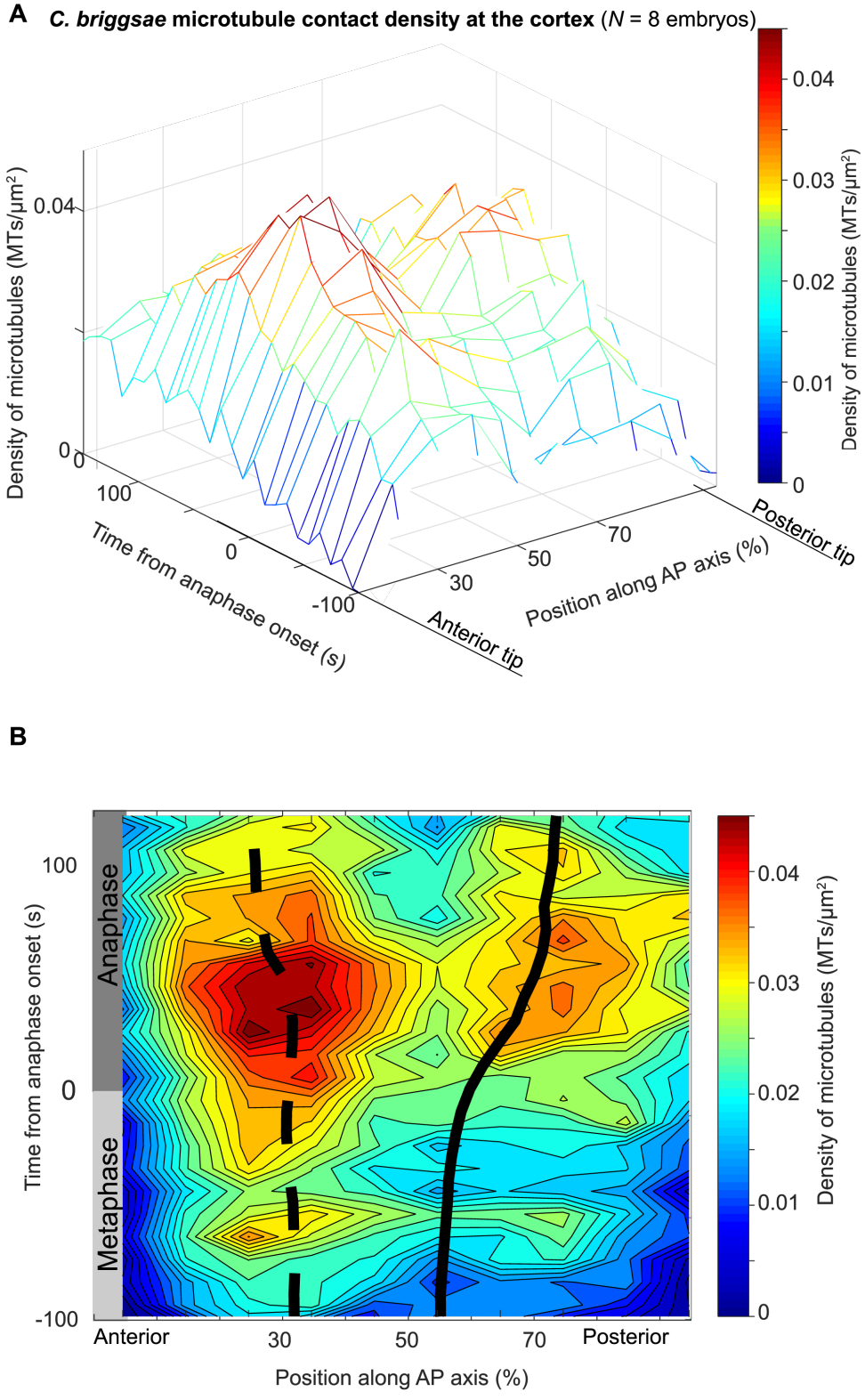

Figure S2: Microtubule contact density at the cell cortex in *C. briggsae*.
(**A**) Microtubule contact density at the cortex obtained by analysing spinning disk microscopy images of the GFP::β-tubulin-labelled microtubule strain of *C. briggsae* (see Methods). The densities were averaged across time (10-seconds window) and position along the anteroposterior (AP) axis using 10 regions of equal width (N = 7 embryos). (**B**) The same microtubule contact density represented by a heat map. The centrosome trajectories were obtained by imaging the γ-tubulin::GFP-labelled centrosome strain (N = 8 *C. briggsae* embryos) on the spindle plane then superimposed on the density map. The dashed line represents the anterior centrosome trajectory, and the solid line is the posterior one.

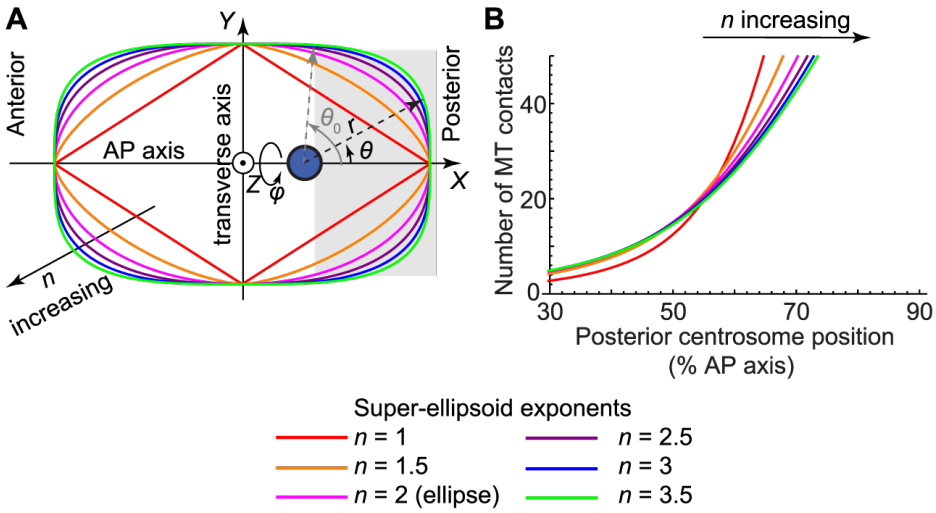

Figure S3: The switch-like behaviour of microtubule contacts is preserved after super-ellipsoid modelling of embryo shape using various exponents. An embryo shape was modelled by super-ellipsoids of the variable *n* (long axis 24.6 µm and short axis 15.75 µm) (Supplementary Text 2.2.3), with *n* = 2 representing the ellipse. **(A)** Super-ellipses with the exponent *n* set to 1 to 3.5. The centrosome was positioned at 67% of the anteroposterior (AP) axis and is a blue disk. Cartesian axes (*X,Y,Z*) are indicated as well as spherical coordinates centered on the centrosome (r,θ,ϕ). The active region is grey, and its boundary was set to 70% of embryo length and at angle θ_0 in centrosome-centered spherical coordinates. **(B)** Number of microtubules contacting the active region *versus* the position of the posterior centrosome along the AP axis, which is shown as a percentage of embryo length. Embryo shape was modelled using super-ellipsoids of revolution based on the super-ellipses plotted in A, and the parameters used are listed in Supplementary Text 4.

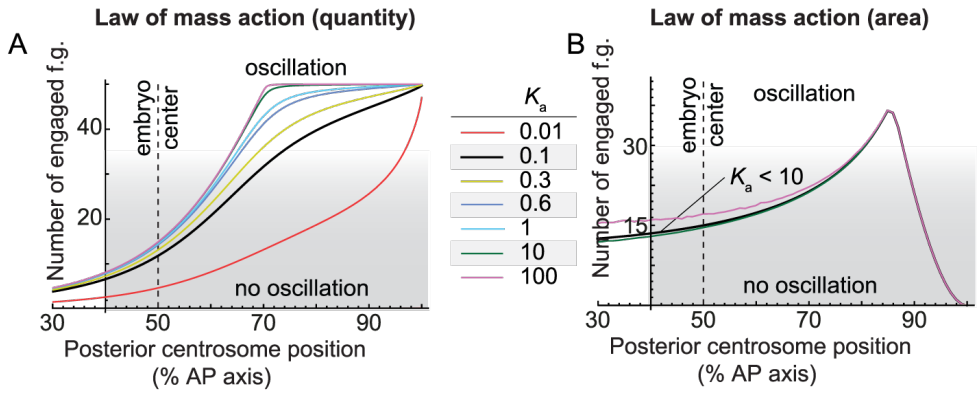

Figure S4: Comparison of law of mass action models using quantity and areal concentrations. When varying the force generator-microtubule association constant K_a, graph of the number of engaged force generators (f.g.) versus the posterior displacement of the centrosome along the anteroposterior (AP) axis (Supplementary Text 2.2.2). For the centrosome positions above 60% of the AP axis, the number of engaged f.g. steeply increases, saturating above 70% and creating a switch-like behaviour. Force generator-microtubule binding was modelled by the law of mass action in: **(A)** quantity, with total number of force generators $N = 50$; and **(B)** areal concentration (Supplementary Text 2.2.2), with $N = 500$. In both cases, we got similar numbers of engaged force generators between 10 to 100 that are consistent with experimental estimates (Grill et al., 2003) (Supplementary Text 2.2.4). The parameters used are listed in Supplementary Text 4. Grey shading indicates when the engaged force generator count was too low to permit oscillation (below threshold).

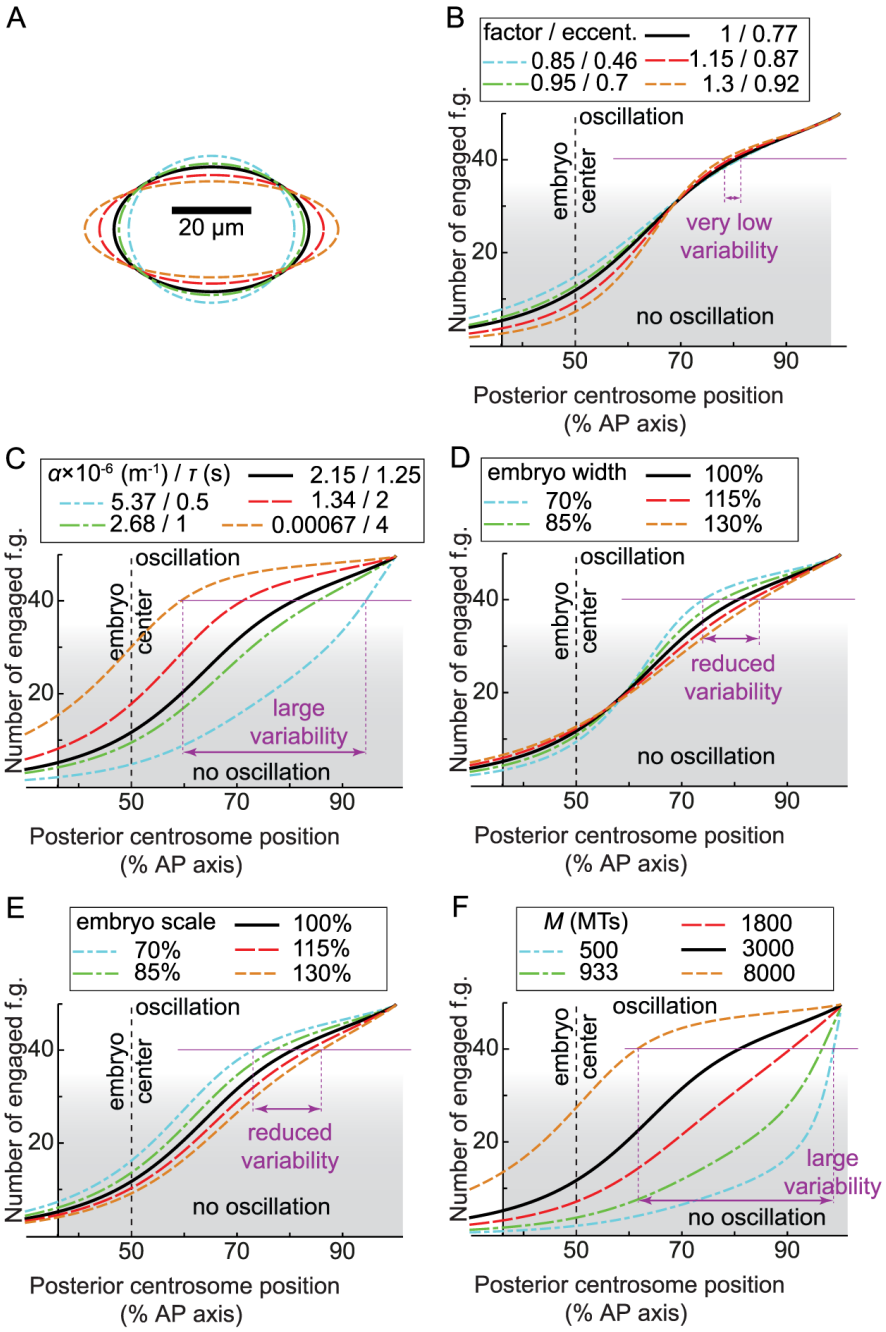

Figure S5: Oscillation onset sensitivity analysis of the expanded "tug-of-war" model. Number of engaged force generators (f.g.), versus the posterior displacement of the centrosome along the anteroposterior (AP) axis. **(A-B)** Variations in the embryo shape after scaling its length by a multiplicative factor and the width by the square root of inverse of this same factor, with the ellipse eccentricity shown in panel A. Doing so, the ellipsoid of revolution modelling the embryo keeps the same volume. **(C)** Variations in microtubule dynamics summarized by parameter α in m^{-1} and its equivalent cortical residency time τ in second, assuming constant growth and shrinkage rates (Supplementary Text 2.1.2). **(D)** Embryo width variations expressed as a percentage of the control. **(E)** Variations in embryo scale factor on length and width (keeping proportions). **(F)** Variations in total number of microtubules M emanating from a single centrosome. In all cases, control values are black; green and blue are lower values; and red and orange are higher ones. The parameters used are listed in Supplementary Text 4. Grey shading indicates when the number of engaged force generators was too low to permit oscillation (below threshold). Purple thin lines, of equal length in each panel, give a variability scale.

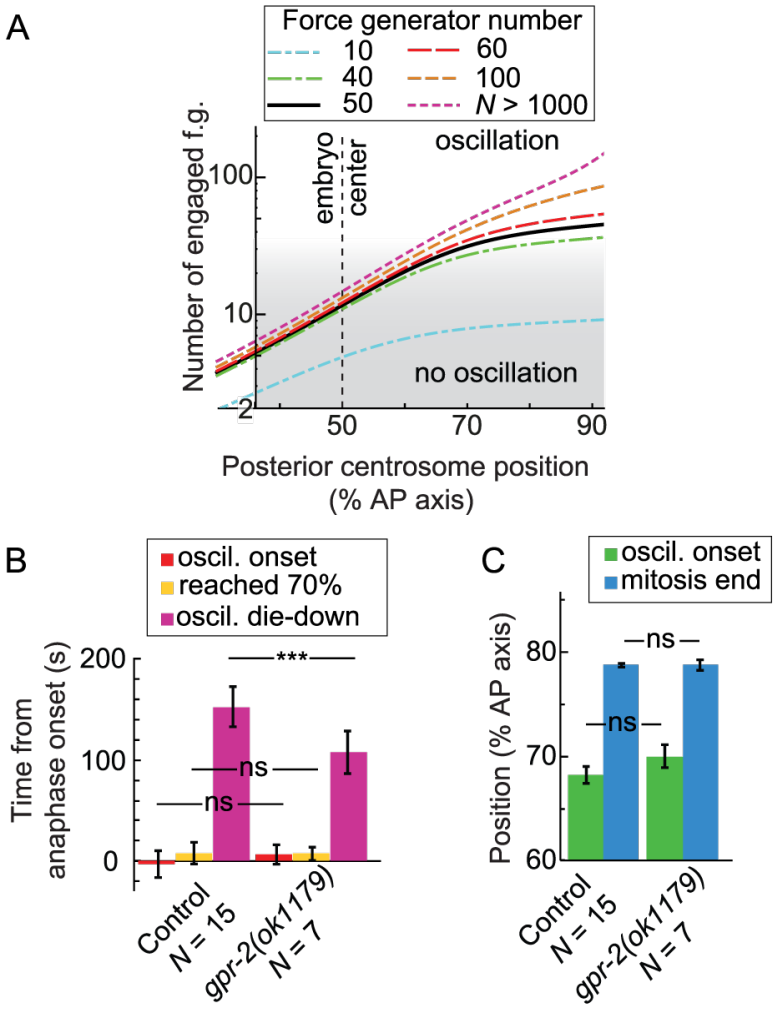

Figure S6: Force generator quantity does not affect the setting of the positional switch. (A) Modelled number of engaged force generators (f.g.) *versus* the posterior displacement of the centrosome along the anteroposterior (AP) axis as a percentage of the embryo length. The number of force generators available is indicated by the colour, with the untreated embryo black, and the *gpr-2(ok1179)* mutant green. The parameters used are listed in Supplementary Text 4. Grey shading indicates when the number of engaged f.g. was too low to permit oscillation (below threshold). **(B)** Timings of oscillation onset, die-down, and when the posterior centrosome reached 70% of AP axis; and **(C)** the posterior centrosome positions of oscillation onset and die-down upon depletion of active f.g. in *gpr-2(ok1179)* mutants (N = 7) compared to N = 15 untreated embryos, both with GFP::γ-tubulin labelling of the centrosome. Error bars indicate SD and stars indicate significant differences (see Methods). All experiments were performed at 18ºC.

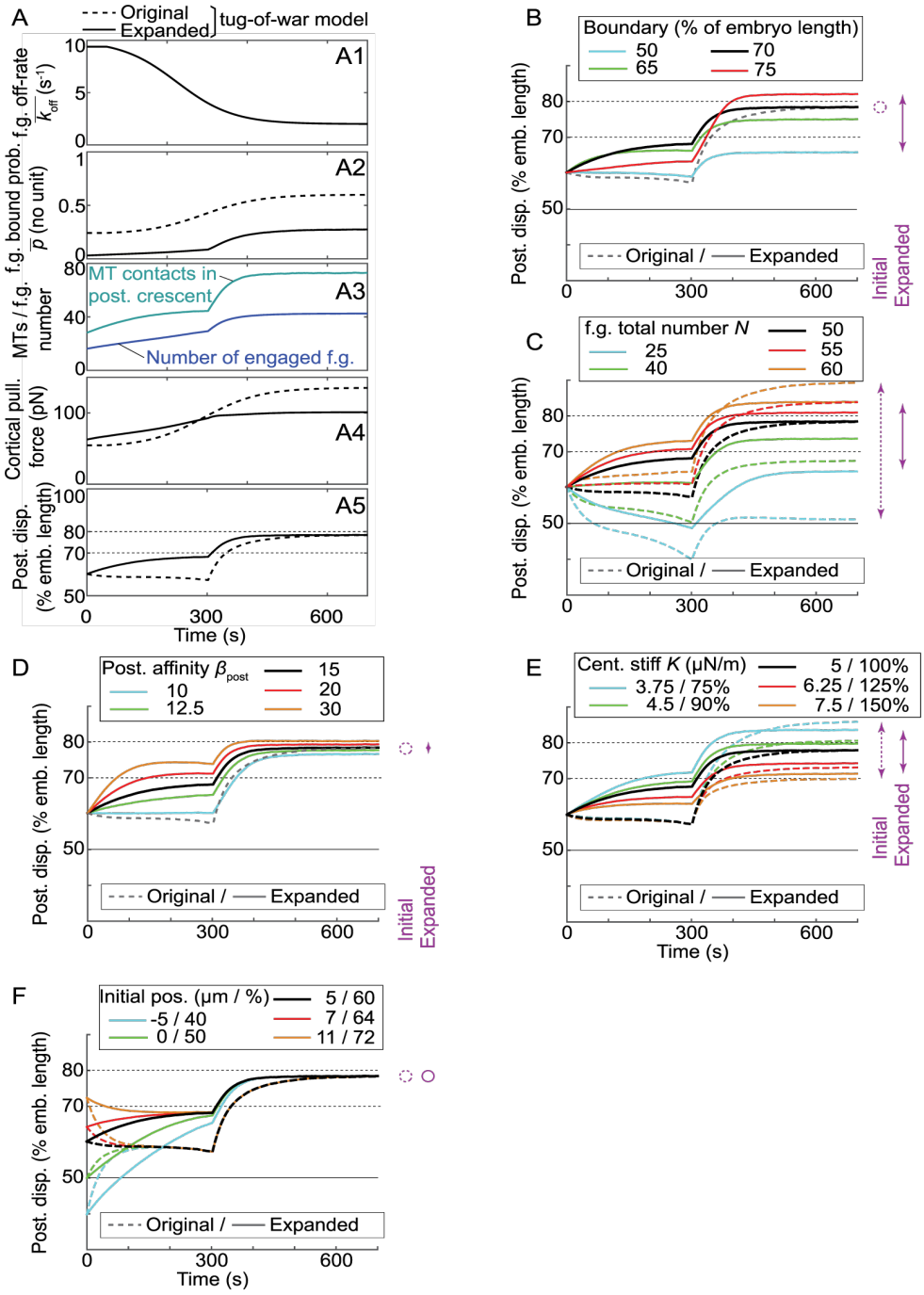

Figure S7: Final position sensitivity analysis of the expanded model. Stochastic simulations of the posterior centrosome displacement. Dashed lines represent the results of the original model, while solid lines correspond to the expanded one (Supplementary Text 3). **(A)** Typical run showing from *top* to *bottom*: (A1) the force generator (f.g.) detachment rate, which is the control parameter encoding the progression through mitosis (Pecreaux et al., 2006); (A2) the probability $\overline{p}$ for a force generator to be bound; (A3) the number of astral microtubules (MTs) contacting the cortex in the posterior crescent (green) and the number of engaged f.g. in this same region (blue); (A4) the cortical force in pN exerted by these f.g. on the posterior centrosome; and (A5) the posterior displacement subsequently obtained. **(B-F)** Posterior displacement of the posterior centrosome averaged over 25 simulation runs with respectively varied: (B) the boundary of the posterior crescent (active region) as a percentage of embryo length; (C) the total f.g. quantity N available per half embryo; (D) the posterior affinity of the f.g. for microtubule (on-rate) varying β, whose asymmetry may encode the polarity (see Supplementary Text 3 after Rodriguez Garcia et al. 2017); and (E) the initial position of the posterior centrosome. When it does not depend on the parameter considered, the original model is shown by a grey dashed line. In all cases, the control values are black; lower values are blue and green; and the higher values are red and orange. The dispersions of the final values for each case are represented by purple arrows, and a larger span in the plot reveals a lack of robustness to parameter variations. A circle is used when the parameter has no effect on the final value. The parameters used are listed in Supplementary Text 4.

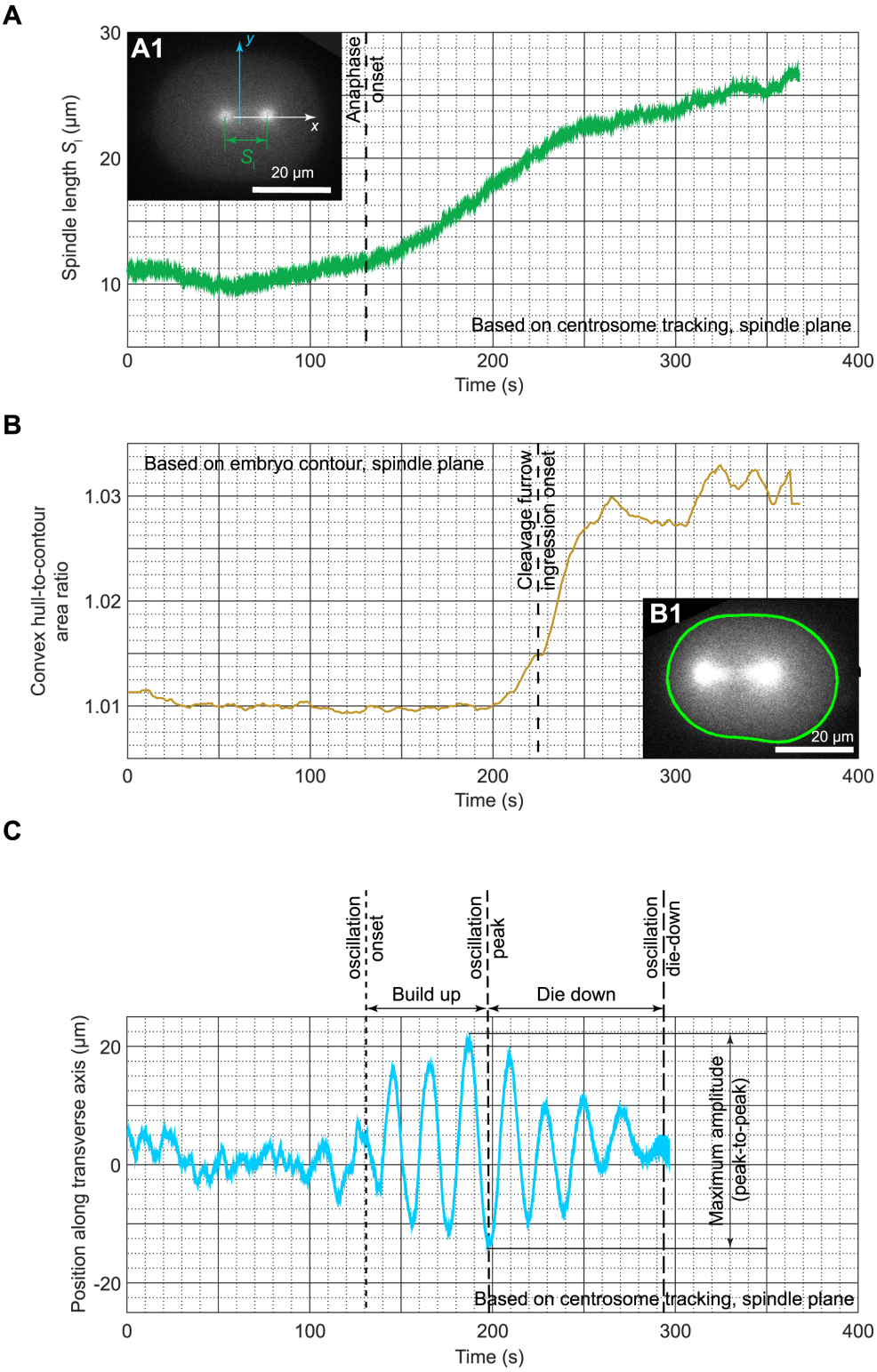

Figure S8: Landmarks used to set reference times and oscillation characteristics. *C. elegans* centrosome trajectories and embryo shapes were measured in the spindle plane by viewing the α-tubulin::YFP-labelled microtubule strain (inset A1). (**A**) The spindle length was measured as the distance between the two centrosomes. Anaphase onset (dashed line) was defined as the inflection point towards a steeper increase in spindle length. (**B**) The ratio of the convex contour to the active contour is related to the convexity of the embryo contour (inset B1; see Supplementary Experimental Procedures) and plotted across time. The cleavage furrow ingression timing (dashed line) is set as the inflection point in the convex hull-to-contour ratio steep increase. (**C**) Position of the posterior centrosome along the transverse axis of the embryo. The timings for the oscillation onset, peak amplitude, and die-down are delineated. The vertical arrow indicates the maximum amplitude measurement (i.e. peak-to-peak distance in consecutive extrema).

Supplementary Experimental Procedures

"Landing" assay: Pipeline to measure microtubule contact densities and dynamics at the cortex

Choosing the strain

Instead of labelling the microtubule +TIPs with EB homolog proteins, we used nematode strains with the entire microtubules labelled with YFP::α–tubulin and GFP::tubulin transgenes for *C. elegans* and *C. briggsae* embryos, respectively. There were two advantages to this: (1) unlike the overexpression of EB proteins[1, 2], this labelling preserved the microtubule dynamics; and (2) it allowed us to measure the duration of the residency of microtubules themselves at the cortex, not just the time spent growing there, which is substantially different[3].

Preprocessing of the cortical images

Since microtubule tubulin spot signals were very weak at the cortex, we denoised the images to increase the signal-to-noise ratio (SNR). This noise reduction usually relies on the assumption that the noise is non-correlated in space and time and that it follows a Gaussian or Poisson distribution over space or time. We opted for Kalman filtering/denoising[4], setting the gain to 0.5, and the initial noise estimate to 0.05 performing in time and not requiring hypothesis in space.

Automated tracking of YFP::α-tubulin fluorescent spots at the cortex

Because of the low SNR and the large quantity of tracks present at the cortex, we looked for an algorithm with powerful track detection and segment linking capabilities. We opted for u-track[5], using the parameters in the table below. We validated these parameters by analysing fabricated images of known dynamics. We were able to find a good co-localization of the simulated tracks and the ones recovered through analysing images fabricated based on the same simulated tracks. We also measured similar lifetimes for both. Because we were conservative in our u-track algorithm parameters, we may have missed some tracks which had low fluorescent intensities.

Detection	
Gaussian standard deviation	1.4
Alpha-value for initial detection of local maxima	0.08
Rolling window time-averaging	3
Iterative Gaussian mixture-model fitting	0
Tracking	
Maximum gap to close	5
Merge split	0
Minimum length of track segments from first step	3
Cost function frame-to-frame linking	
Flag for linear motion Allow instantaneous direction reversal	1 1
Search radius lower limit	1
Search radius upper limit	3
Standard deviation multiplication factor	3
Nearest neighbor distance calculation	1

Number of frames for nearest neighbor distance calculation	4
Cost function close gaps	
Flag for linear motion	1
Search radius lower limit	1
Search radius upper limit	3
Standard deviation multiplication factor	3
Nearest neighbor distance calculation	
Number of frames for nearest neighbor	4
Penalty for increasing gap length	1.5
Maximum angle between linear tracks segments	30

Measuring microtubule residency time at the cortex

We calculated the histogram for the durations of microtubule contacts at the cortex. We used a bin size of 100 ms, equal to the image acquisition time. The exponential fit of the histogram yielded a microtubule lifetime of about 1 s (Fig. S1B), consistent with previous work[3].

Computing microtubule contact densities at the cortex

The "landing" assay consisted of measuring the cortical microtubule contacts (Fig. S1A) during the different phases of mitosis. The part of the embryo contacting the cover-slip was divided into ten regions of equal width along its long axis (AP axis). The u-track algorithm allowed us to follow the microtubule contacts at the cortex frame-by-frame, and to have access to their trajectories[5]. We segmented the embryo cytoplasm so we could track embryo shape changes throughout cell division using the active contour algorithm[6], thus obtaining data on how the lengths and areas of the embryos evolved during mitosis. We were then able to count the microtubules contacting the cortex in the ten regions along the embryo length (Fig. S1A). To reinforce our findings, the distribution of the microtubule contacts was averaged over time for 10 s. Finally, we used the onset of cytokinesis cleavage furrow ingression as a temporal reference for the alignment of the different microtubule cortical contact density maps, then averaged the embryos to get the final density map.

Timing of cytokinesis cleavage furrow ingression onset to overlay centrosome trajectories to microtubule contact density

We determined the timing of the onset of cleavage furrow ingression in both planes by taking advantage of the dyed cytoplasmic fraction to detect the embryo contours. These contours were obtained via the active contour algorithm[6]. We then set the onset of cleavage furrow ingression to equal the fast increase in embryo shape convexity (or the ratio of the convex area to the active contour one) (Fig. S8B), which in practice meant when it grew above 1.012. In the midplane, we calibrated the average time between anaphase (starting at the inflection point during spindle elongation[7], Fig. S8A) and the onset of cleavage furrow ingression. We then used this to estimate anaphase onset from cortical cleavage furrow ingression onset measurements, matching the timing from the "landing" and "centrosome-tracking" assays to plot overlays (Fig. 1 and S2B).

Robustness plot (Fig. 4)

To assess the robustness of the positions of the posterior centrosomal oscillation onset and die-down and of the timing of the oscillation onset against embryo length variations, we used dimensionless quantities. For the timing, we used the reference duration T equals to the delay between two mitotic events independent of cell mechanics for control embryos. We chose the Nuclear Envelope BreakDown (NEBD) and the anaphase onset. For each experiment, we computed t_0, the shift of the oscillation onset time with respect to the anaphase onset. The normalized shift $\overline{\delta t_0}$ was thus obtained by subtracting the corresponding mean value for control t_0^{ctrl} from the current value t_0, and by dividing the result by the reference duration: $\overline{\delta t_0} = \left(t_0 - t_0^{ctrl}\right)/T$. We repeated this

calculation for the positional quantities using the control's mean embryo length L as a reference for normalization. For each experiment, we computed the shift of the position of oscillation onset, p_0, or of oscillation die-down, p_d, with respect to the corresponding control mean position p_o^{ctrl} or p_d^{ctrl}, respectively. Normalization yielded the normalized shift of the oscillation onset $\overline{\delta p_0} = \left(p_o - p_o^{ctrl}\right)/L$ and of their die-down $\overline{\delta p_d} = \left(p_d - p_d^{ctrl}\right)/L$. Independently of the quantity used for normalizing, we used a Student's *t*-test to see whether the linear fit slope was significantly different from 0. In doing so, we were able to determine whether e.g. embryo length had an impact on the positions or timing being studied, since both the means and corresponding standard deviations scaled identically when using this normalizing factor.

References

1. Straube A, Merdes A. EB3 regulates microtubule dynamics at the cell cortex and is required for myoblast elongation and fusion. *Curr Biol* **17**, 1318-1325 (2007).

2. Komarova Y*, et al.* Mammalian end binding proteins control persistent microtubule growth. *J Cell Biol* **184**, 691-706 (2009).

3. Kozlowski C, Srayko M, Nedelec F. Cortical microtubule contacts position the spindle in C. elegans embryos. *Cell* **129**, 499-510 (2007).

4. Kalman RE. A New Approach to Linear Filtering and Prediction Problems. *Journal of Basic Engineering* **82**, 35-45 (1960).

5. Jaqaman K*, et al.* Robust single-particle tracking in live-cell time-lapse sequences. *Nat Methods* **5**, 695-702 (2008).

6. Pecreaux J, Zimmer C, Olivo-Marin JC. Biophysical active contours for cell tracking I: Tension and bending. In: *2006 Ieee International Conference on Image Processing, Icip 2006, Proceedings* (ed^(eds) (2006).

7. Pecreaux J*, et al.* The Mitotic Spindle in the One-Cell C. elegans Embryo Is Positioned with High Precision and Stability. *Biophys J* **111**, 1773-1784 (2016).

Supplementary text for the article "Microtubule dynamics regulate anaphase oscillation onset and the final spindle position in the nematode zygote."

Hélène Bouvrais[*,1,2], Laurent Chesneau[1,2], Sylvain Pastezeur[1,2], Marie Delattre[3], and Jacques Pécréaux[*,1,2]

[1]CNRS UMR 6290, F-35043 Rennes, France.
[2]University of Rennes 1, UEB, SFR Biosit, School of Medicine, F-35043 Rennes, France
[3]Laboratory of Molecular Biology of the Cell, École Normale Supérieure de Lyon, CNRS, F-69363 Lyon, France

April 5, 2017

[*]To whom correspondence should be addressed: helene.bouvrais@univ-rennes1.fr, jacques.pecreaux@univ-rennes1.fr (Lead Contact)

Contents

1 Introduction

We aimed to complement our previously published "tug-of-war" model (Grill et al., 2005; Pecreaux et al., 2006), mainly focused on the dynamics of cortical force generators (f.g.), by including the dynamics of astral microtubules (MTs). Indeed, we mapped the microtubule contacts at the cortex and revealed that they mostly concentrated in cortical regions close to the centrosomes (Fig. 1). In consequence, the position of the centrosomes, as microtubule organizing centres (MTOC), regulates through the microtubule dynamics the quantity of engaged force generators, likely cytoplasmic dynein (Nguyen-Ngoc et al., 2007), pulling on astral microtubules. In turn, this regulates anaphase spindle oscillations and posterior displacement. First, focusing on the oscillation onset, we expanded our initial model of spindle oscillation to account for microtubule dynamics. We will detail the expanded model and then explore how this novel positional regulation combines with the one by force generator processivity previously reported (Pecreaux et al., 2006). In that case, we assumed that the change in force generator processivity throughout mitosis was negligible. Second, through a stochastic simulation approach, we looked at the feedback loop created between the position of the posterior centrosome and the pulling forces contributing to spindle displacement. In this case, we considered the variations in force generator processivity, possibly linked to the cell cycle.

2 Modelling the positional switch on oscillation onset

2.1 Quantity of microtubules reaching the posterior crescent of active force generators

Recent work suggested that force generators would be active only on a posterior cap instead of the whole posterior half cortex of the embryo (Krueger et al., 2010). This means that only the microtubules hitting the posterior crescent of the cortex would contribute to spindle displacement by binding to pulling force generators. We thus calculated the number of microtubules reaching this so-called active region of the cortex.

2.1.1 Modelling hypotheses and microtubule dynamics parameter estimates

We set to explore whether the number of microtubules reaching the cortex, assumed to be in excess during anaphase (Grill et al., 2005; Pecreaux et al., 2006), could be limiting prior to oscillation onset. Key to assess this possibility was an estimate of the total number of microtubules and their dynamics. Based on previously published experiments, we assessed the following microtubule related parameters:

- **Total number of microtubules.** To assess the number of microtubule nucleation sites at the centrosome (CS), we relied on electron microscopy images of the centrosomes (Redemann et al., 2016), which suggested 3000 or more microtubules emanating per centrosome. This order of magnitude was previously proposed by O'Toole and collaborators (O'Toole et al., 2003). More specifically in the figure 3, authors provide a

slice of about 0.85 μm thick (as estimated from video 8) displaying 520 astral microtubules, while centrosome diameter was estimated to 1.5 μm. Only a slice of centrosome was viewed in this assay, so that the number of microtubule nucleation sites per CS was estimated to a least 1800 considering the centrosome as a whole sphere. In this work, we set the number of microtubules to $M = 3000$. Variation of this number within the same order of magnitude does not change our conclusions.

- **The microtubules are distributed around each centrosome in an isotropic fashion.** We hypothesized an isotropic distribution of microtubules around each centrosome following (Howard, 2006). This was also suggested through electron microscopy (Redemann et al., 2016).

- **Free-end catastrophes are negligible.** With the above estimate of the microtubule number and considering a microtubule growing speed in the cytoplasm $v^+ = 0.67$ μm/s (Srayko et al., 2005) and a shrinking one $v^- = 0.84$ μm/s (Kozlowski et al., 2007), we could estimate that about 70 microtubules reach the cell periphery (assumed to be at 15 μm from the centrosome) at any moment and per centrosome, if the free-end catastrophe rate is negligible. This estimate appear consistant with the instantaneous number of force generator in an half-cortex, estimated between 10 and 100 (Grill et al., 2003).

  Recently, it was proposed that the catastrophe rate could be as high as 0.25 s^{-1} in the mitotic spindle (Redemann et al., 2016). On the one hand, this might be specific to this organelle since the spindle is much more crowded than the cytoplasm. On the other hand, these authors proposed a total number of microtubules two to three folds larger than our estimate. We asserted that our conservative estimate of the microtubule quantity combined with the negligible free-end catastrophe resulted in similar modelling results, with the advantage of the simplicity over a full astral microtubule model. In other words, we focused on the fraction of astral microtubules not undergoing free-end catastrophe, which was the only one measurable at the cortex.

  We next wondered whether the assumption of negligible free-ends catastrophe is consistent with our measurement of microtubule contact density at the cortex. After (Redemann et al., 2016), the vast majority of microtubules emanating from the centrosome are astral: we thus assumed that the kinetochore and spindle microtubules were negligible in this estimate. Focusing on metaphase and with a residency time of microtubule ends at the cortex $\tau = 1.25$ s (this work and (Kozlowski et al., 2007)), this led to about 100 microtubules contacting the cortex per centrosome, at any given time. Using our "landing" assay (Supplementary Fig.s S1C, S2A), we could estimate the number of contacts in the monitored region at any given time to 5 microtubules. Extrapolating this to a whole centrosome and assuming the isotropic distribution of astral microtubules (§2.1.2), we found 26 cortical contacts of microtubules at any time in metaphase. Although a bit low, likely because of the conservative parameters of the image processing (Supplementary Experimental Procedures) that could lead to missing some microtubules, this estimate was consistent with the estimate based on our hypotheses. Furthermore, it is also consistent with the measurement done by (Garzon-Coral et al., 2016). In contrast, a non negligible catastrophe rate would have dramatically reduced that number of contacts at any given time. We concluded that free-end catastrophe rate was safely negligible.

- **No microtubule nucleation sites are left empty at the centrosomes** This is a classic hypothesis (Howard, 2006), recently supported by electron microscopy experiments (Redemann et al., 2016).

2.1.2 Microtubule dynamics "measure" the centrosome-cortex distance.

Probability for a microtubule to be at the cell cortex Because microtubules spend most of their "lifespan" growing to and shrinking from the cortex, the distance between the centrosome and the cortex limits the number of microtubules residing at the cortex at any given time. We could thus summarize microtubule dynamics in a single parameter α by writing the fraction of time spent by a microtubule at the cell cortex:

$$q \;=\; \frac{\tau}{\frac{d}{v^+}+\frac{d}{v^-}+\tau} \;=\; \frac{1}{1+\alpha d} \quad \text{with } \alpha = \frac{1}{v^+\tau}+\frac{1}{v^-\tau}, \tag{1}$$

where d is the distance from the centrosome (MTOC) to the cortex (estimated to typically $d = 15$ μm, *id est* about half of the embryo width). We then found $\alpha = 2.15 \times 10^6$ m^{-1} using the above microtubule dynamics parameters. This meant that the microtubule spent $q = 3\%$ of its time at the cortex and the remaining time growing and shrinking. This fraction of time spent residing at the cortex was consistent with the estimate coming from investigating the spindle centering maintenance during metaphase (Pecreaux et al., 2016).

Range of variations in the microtubule contact densities at the cortex. The nematode embryo shape is slightly elongated. Therefore, the centrosome displacement can vary the centrosome-cortex distance by 1.5 to 2 fold. We wondered whether the microtubule dynamics were so that one could observe significant variations in cortical microtubule-residing probabilities q. We estimated this sensitivity through the ratio ρ of the probability of reaching the cortex when the centrosome was at its closest position d_1 (set to half of the embryo width, i.e. the ellipse short radius) divided by the probability when it was at its furthest position d_2 (chosen as half of the embryo length, i.e. the ellipse long axis).

$$\rho = \frac{1+\alpha d_2}{1+\alpha d_1} \tag{2}$$

This curves had a sigmoid–like shape with $\lim_{\alpha\to 0}\rho = 1$ and $\lim_{\alpha\to\infty}\rho = d_2\,/d_1\,$.

Using our measurement of microtubule contact distribution at the cortex (Supplementary Fig. S1C, S2A), we calculated an experimental estimate of this sensitivity parameter. However, because our assay did not enable us to view the very tip of the embryo (Supplementary Fig. S1A), we compared the sensitivity ratio calculated from the density map with a theoretical one that did not use the half embryo length as maximum distance but the largest distance effectively measurable. For untreated embryos viewed at the spindle plane, the measured embryo length was $2a = 49.2$ μm, while imaging at the cortex, the length along anteroposterior (AP) axis (denoted with bars) was $2\bar{a} = 38.0$ μm for the adhering part to the coverslip (Supplementary Fig. S1A). We could calculate the truncation of the ellipse due to the adhesion through the polar angle $\zeta = \arccos(\bar{a}\,/a\,)$ of the boundary of the adhering region. We obtained $\zeta = 39.4°$ which corresponded to a spindle plane to flattened cortex distance of 10 μm,

using a parametric representation of the ellipse. During metaphase (set as the two minutes preceding anaphase onset), when the spindle is roughly centered (Pecreaux et al., 2016), the average spindle length was 11.8 μm ($N = 8$ embryos). The furthest visible region was thus at $d_2 = 16.5$ μm while the closest one was at $d_1 = 10$ μm, leading to a sensitivity ratio $\rho = 1.62$ consistent with the microtubule cortical contact density ratio observed *in vivo* for *C. elegans* (Fig. 1, S1C). We concluded that microtubule dynamics in *C. elegans* enable the read-out of the posterior centrosome position through the probability of microtubules to be in contact with the cell cortex.

2.1.3 Number of microtubules reaching the cortex

We set to estimate the variation of the total number of astral microtubule contacts emanating from a single centrosome versus the position of this centrosome along the AP axis. We worked in spherical coordinates (r, θ, ϕ) centered on the posterior centrosome that displayed a slow posterior displacement assumed to be a quasi-static motion, with zenith pointing towards posterior. We denoted θ the zenith angle and ϕ the azimuth (Supplementary Fig. S3A). We calculated the probability of a microtubule to reach the cortex in the active region, represented as $\theta \in [0, \theta_0]$ and $\phi \in [0, 2\pi[$. We integrated over the corresponding solid angle. Then the number of microtubules reaching the cortex $\mathcal{M}(\mathcal{S}, \alpha)$ comes readily (Fig. 2A):

$$p(\mathcal{S}, \alpha, \theta, \phi) = \frac{1}{1 + \alpha\, r_{\mathcal{S}}(\theta, \phi)} \sin(\theta) \tag{3}$$

$$P(\mathcal{S}, \alpha) = \int_{\theta=0}^{\theta_0} \int_{\phi=0}^{2\pi} p(\mathcal{S}, \alpha, \theta, \phi)\, \mathrm{d}\,\phi\, \mathrm{d}\,\theta \tag{4}$$

$$\mathcal{M}(\mathcal{S}, \alpha) = M / 4\pi\; P(\mathcal{S}, \alpha) \tag{5}$$

where $r_{\mathcal{S}}(\theta, \phi)$ is the distance centrosome-cortex in polar coordinates centered on the centrosome, dependent upon the shape of the cortex $\mathcal{S}$ and the boundary of the active force generator region θ_0 (Fig. 2C). We observed a switch-like behaviour as the posterior centrosome went out of the cell centre and closer to the posterior side of the embryo (Fig. 2A).

2.2 The expanded tug-of-war model

In the initial model (Grill et al., 2005; Pecreaux et al., 2006), we made the assumption that the limiting factor was the number of engaged cortical force generators while in comparison, the astral microtubules were assumed to be in excess. It resulted that oscillations were driven by the force generator quantity and dynamics. In the linearised version of the initial model, the persistence of force generators to pull on microtubules (i.e. their processivity) mainly governed the timing and frequency of the oscillations, while the number of force generators drove the amplitude of oscillations (Pecreaux et al., 2006). However, since the number of microtubules reaching the cortex could be limiting (Kozlowski et al., 2007), we expanded the initial model of anaphase oscillations to account for this possible limitation.

2.2.1 The initial model

We provide here a brief reminder of the previously published tug-of-war model (Pecreaux et al., 2006). This model featured cortical force generators exhibiting stochastic binding to and detaching from microtubules at rates k_{on} and k_{off} ($\overline{k_{off}}$ being the detachment rate at stall force $\bar{f}$), respectively. The probability for a force generator to be pulling on a microtubule then reads $\bar{p} = k_{on} \big/ \left(k_{on} + \overline{k_{off}}\right)$. The active force generators were distributed symmetrically between the upper and lower posterior cortices (the case developed here) but asymmetrically between anterior and posterior cortices (Grill et al., 2003) (§2.2.2). In the model, we also included two standard properties of the force generators: firstly, a force-velocity relation $f = \bar{f} - f'\,v$, with f the current force, v the current velocity, and f' the slope of the force velocity relation ; secondly, a linearised load dependent detachment rate $k_{off} = \overline{k_{off}} \left(1 - \frac{\bar{f}-f}{f_c}\right)$, with f_c the sensitivity to load/pulling force, assuming that force generator velocity was low, i.e. they acted close to the stall force (Pecreaux et al., 2006). We finally denoted Γ the passive viscous drag, related in part to the spindle centering mechanism (Garzon-Coral et al., 2016; Howard, 2006; Pecreaux et al., 2016) and $\bar{N}$ the number of available force generators in the posterior cortex.

A quasi-static linearised model of the spindle posterior displacement reads:

$$I(\bar{p})\ddot{y} + \left(\Gamma - \Xi(\bar{p})\right)\dot{y} + Ky = 0, \tag{6}$$

with

$$\Xi(\bar{p}) = 2\bar{N}\left\{\frac{\bar{f}}{f_c}\bar{p}\left[(1-\bar{p}) - \frac{f_c}{\bar{f}}\right]\right\} f', \tag{7}$$

and

$$I(\bar{p}) = 2\bar{N}\left\{\frac{\bar{f}}{f_c}\bar{p}\,(1-\bar{p})\right\} f'\frac{\bar{p}}{k_{on}}, \tag{8}$$

with K the centering spring stiffness and I the inertia resulting from stochastic force generator binding and unbinding. The spindle oscillations develop when the system become unstable, meaning when the negative damping $\Xi(\bar{p})$ overcomes the viscous drag Γ.

2.2.2 Evolution of the initial model to account for the polarity encoded through force generator on-rate

When we designed the initial model, it was known that the spindle posterior displacement was caused by an imbalance in the number of active force generators (Grill et al., 2003), i.e. the number of force generator engaged in pulling on astral microtubules. However, the detailed mechanism building this asymmetry was elusive. We recently investigated the dynamics of dynein at the cell cortex (Rodriguez Garcia et al., 2017) and concluded that an asymmetry in force generator attachment rate to the microtubule together with the remaining components of the trimeric complex (Nguyen-Ngoc et al., 2007). This asymmetry reflects the asymmetric location of GPR-1/2 (Park and Rose, 2008; Riche et al., 2013). More abundant GPR-1/2 proteins at posterior cortex could displace the attachment reaction towards more binding/engaging of force generators. Therefore, to simulate the posterior displacement of the posterior centrosome (§3), we rather used the equations above (Eq. 6-8) with distinct on-rates between anterior and posterior sides and equal quantity of available force generators.

2.2.3 Number of engaged force generators: modelling the binding of a microtubule to a force generator

To account for the limited number of cortical anchors (Grill et al., 2005; Pecreaux et al., 2006), we modelled the attachment of a force generator to a microtubule (Nguyen-Ngoc et al., 2007) as a first order process, using the law of mass action on component quantity (Koonce and Tikhonenko, 2012) and combined it to the equations of quantity conservation for force generators and microtubules.

Force generator–Microtubule attachment modelling

$$K_a = \frac{N_{\text{microtubule–force-generator}}}{N_{\text{free-microtubule-at-cortex}}\, N_{\text{free-force-generator}}} \tag{9a}$$

$$N = N_{\text{Microtubule–force-generator}} + N_{\text{free-force-generator}} \tag{9b}$$

$$M = N_{\text{microtubule–force-generator}} + N_{\text{free-microtubule-at-cortex}} \tag{9c}$$

$$= \mathcal{M}(\mathcal{S}, \alpha) \tag{9d}$$

where N is the total number of force generators present in the active region.

We could relate the association constant K_a to our previous model (Pecreaux et al., 2006) (§2.2.1) by writing

$$K_a = \begin{cases} \widehat{k_{on}} \,/\overline{k_{off}} \\ \\ \bar{p}\,/(1-\bar{p})\,/N_{\text{free-microtubule-at-cortex}} \end{cases} \tag{10}$$

with the on-rate $k_{on} = \widehat{k_{on}} N_{\text{free-microtubule-at-cortex}}$, and the off-rate $\overline{k_{off}}(t)$ thought to depend on mitosis progression. Time dependences were omitted for sake of clarity. It is noteworthy that k_{on}, used in the initial model as force generator binding rate (assuming microtubules in excess), became variable throughout mitosis in the expanded model as it depends on the number of free microtubule contacts at the cortex, thus on the centrosome position. In contrast, $\widehat{k_{on}}$ appeared constant in the expanded model representing the on-rate of the first order reaction above.

Related parameter estimate In modelling anaphase oscillation onset, we assumed that the off-rate dependence on mitosis progression was negligible (§2.2.6 and 3 for full model without this assumption). The positional switch modelled here led to a limited number of engaged force generators at oscillation onset. At this time, the force generator quantity just crossed the threshold to build oscillations (Pecreaux et al., 2006) and we estimated that 70% of the force generators were thus engaged, consistent with the quick disappearance of oscillations upon progressively depleting the embryo from GPR-1/2 proteins. We observed that the oscillation started when the centrosome reached 71% of embryo length (Table 1). At that moment, 52 microtubules were contacting the cortex (§2.1.1). We set the total number of force generators to 50 and got a number of engaged ones consistent with previous reports

(Supplementary Fig. S6A) (Grill et al., 2003). We thus estimated the association constant $K_a^0 \simeq 0.1$ (denoted with 0 superscript to indicate that we assumed negligible its variation throughout mitosis). In turn, we estimated $\widehat{k_{on}} \simeq 0.025$ s^{-1} assuming that the detachment rate at that time was about 4 s^{-1} (Rodriguez Garcia et al., 2017). If 70% of the force generators were engaged at oscillation onset, it would correspond to $k_{on} \simeq 0.375$ s^{-1}, thus comparable to the estimate used in the initial model (Pecreaux et al., 2006).

Modelling the number of engaged force generators in the posterior crescent In mitosis early stages, when the spindle lays in the middle of the embryo (*C. elegans*) or slightly anteriorly (*C. briggsae*), both centrosomes are far from their respective cortex and thus the imbalance in active force generator quantity due to embryo polarity results in a slight posterior pulling force and causes a slow posterior displacement. The closer the posterior centrosome gets to its cortex, the larger the force imbalance (because more microtubules reach the cortex), and the posterior displacement accelerates to (potentially) reach an equilibrium position during metaphase resulting in a plateau in posterior centrosome displacement located around 70% of the AP axis. Once anaphase is triggered, the decreased coupling between anterior and posterior centrosomes results into a sudden imbalance in favour of posterior pulling forces so that the posterior displacement speeds up.

We quantitatively modelled this phenomenon by combining the law of mass action above (Eq. 9a) with the number of microtubules reaching the posterior crescent (Eq. 5) to obtain the number of engaged force generators in the posterior cortex as following:

$$\begin{aligned} &\mathcal{N}\left(\mathcal{M}\left(\mathcal{S},\alpha\right)\right) = N\frac{\phi-1}{\phi+1} \\ &\quad \text{with} \quad \phi = \zeta^- + \sqrt{1+\zeta^{-2}+2\zeta^+} \\ &\quad \zeta^{\pm} = K_a\left(\mathcal{M}\left(\mathcal{S},\alpha\right) \pm N\right) \end{aligned} \tag{11}$$

To challenge our model, we tested the switch-like behaviour in a broad range of association constants K_a (Supplementary Fig. S4A). When the posterior centrosome was between 50% and 70% of embryo length, we observed that the number of engaged force generators was increased up to a threshold that enabled oscillations, consistently with (Pecreaux et al., 2006). When the centrosome was posterior enough, practically above 70% of AP axis, the number of engaged force generators saturated, suggesting that their dynamics were now the control parameters, as proposed in the initial model during anaphase. We also observed that a minimal binding constant was required to reach the threshold number of engaged force generators required for oscillations. Interestingly, above this minimal K_a, further increase of the binding constant did not alter significantly the positional switch (Supplementary Fig. S4A). This suggested that this positional switch operates rather independently of the force generator processivity. This will be further discussed below (§2.2.6).

The positional switch is independent of the total number of force generators, as soon as this quantity is above a threshold As we previously suggested that the total number of force generators should not impact the positional switch (Riche et al., 2013), we calculated the corresponding prediction in our model (Supplementary Fig. S6A) and looked

for an experimental confirmation. The number of active force generators contributing to the posterior displacement is controlled by GPR-1/2 proteins (Colombo et al., 2003; Grill et al., 2003; Park and Rose, 2008; Riche et al., 2013). To keep above the threshold needed for oscillations (Pecreaux et al., 2006), we only decreased partially the number of active force generators through a mutation of one of their redundant regulators, GPR-2, using a strain carrying both GFP::α-tubulin transgene and *gpr-2(ok1179)* mutation. Oscillation amplitude was decreased to 7.1 $\pm$ 0.9% of embryo width ($N = 8$, $p = 1.47\times10^{-5}$) with respect to control, whose amplitude was 19.2 $\pm$ 0.9% of transverse axis, confirming a reduction in the number of active force generators. In these conditions, we observed that the oscillations still started when the posterior centrosome reached 70% of embryo length (Supplementary Fig. S6C) and slightly later than the control (Supplementary Fig. S6B). This result supports our model, provided that asymmetry of active force generator is modelled following the common thought that GPR-1/2 increase the total number of force generators on the posterior side, and when the total force generator number is above the threshold of the initial model. The centrosome position sets where oscillation starts. We recently proposed that the asymmetry in active force generators could be an asymmetry of force generator association rate to form the trimeric complex that pulls on microtubules (Rodriguez Garcia et al., 2017). GPR-1/2 presence would increase this on-rate. In our expanded model, a decreased on-rate (through *gpr-2* mutant) would result in a decrease association constant K_a. Similarly to the case with an asymmetry in number, above a certain threshold of K_a, the position at which oscillations were set on was not significantly modified (Supplementary Fig. S4A). In conclusion, independently of the details used to model the polarity (i.e. in total number or in on-rate), the mild depletion of GPR-1/2 experiment, causing a reduced number of active force generators, supported our expanded model.

To further understand how the various parameters could impact this switch-like behaviour, we performed a sensitivity analysis of oscillation onset using the revised model (Fig. 2B, 4A, Supplementary Fig. S6A, S4A, S5).

2.2.4 The switch-like behaviour of the number of microtubules reaching the cortex versus the centrosome position is independent of detailed embryo shape

The above results were obtained by assuming an ellipsoidal shape for the embryo (an ellipsoid of revolution around the AP axis, prolate or oblate). We wondered whether a slightly different shape could alter the result. We thus repeated the computation, modelling the embryo shape by a super-ellipsoid of revolution, based on super-ellipses (Lamé curves) (Edwards, 1892) defined as:

$$\left|\frac{X}{a}\right|^n + \left|\frac{Y}{b}\right|^n = 1 \tag{12}$$

with a and b the half length and width, n the exponents, and (X, Y, Z) the cartesian axes with X along the AP axis (long axis), and positive values towards the posterior side. We obtained a similar switch-like behavior (Supplementary Fig. S3). We concluded that the switch-like behavior observed was resistant to changes of the detailed embryo shape and thus we performed the remaining investigations with an ellipsoid shape, for sake of simplicity.

2.2.5 Discussion: number– or density–limited force generator-microtubule binding

By writing the law of mass action in protein quantity (Eq. 9a), we assumed that the force generator-microtubule binding reaction was rate-limited but not diffusion-limited. We recently investigated the dynamics of cytoplasmic dynein (Rodriguez Garcia et al., 2017) and observed that dynein molecules were abundant in cytoplasm, thus 3D diffusion combined to microtubule plus-end accumulation brought enough dynein to the cortex. Therefore, diffusion of dynein to the cortex was not likely to be a limiting factor in binding force generators to the microtubules. However, another member of the force-generating complex, GPR-1/2, essential to generate pulling forces (Grill et al., 2003; Nguyen-Ngoc et al., 2007; Pecreaux et al., 2006), may be limiting. GPR-1/2 is likely localised at the cell cortex prior to assembly of the trimeric complex (Park and Rose, 2008; Riche et al., 2013), and in low amount leading to a limited number of cortical anchors (Grill et al., 2003, 2005; Pecreaux et al., 2006). We thus asked whether a limiting areal concentration of GPR-1/2 at the cortex could alter our model predictions. In the model proposed here, we considered force generator as a reactant of binding reaction. This latter included the molecular motor dynein but also other member of the trimeric complex, as GPR-1/2. Therefore, a limited cortical areal concentration in dynein or GPR-1/2 was modelled identically as a limited areal concentration of force generator. We wrote the corresponding law of mass action in concentration:

$$\tilde{K}_a = \frac{[\text{Microtubule–force-generator}]}{[\text{Microtubule-at-cortex}]\ [\text{force-generator}]}, \tag{13}$$

with $[\text{force-generator}] = \frac{N_{\text{force-generator}}}{S_{activeRegion}}$, $\tilde{K}_a = K_a S_{activeRegion}$ and $S_{activeRegion}$ the posterior crescent surface (active region), whose boundary is considered at 70% of embryo length. Modelling the embryo by a prolate ellipsoid of radii 24.6 μm and twice 15.75 μm, we obtained $S_{activeRegion} \simeq 0.147\, S_{embryo} = 610\ \mu\text{m}^{-1}$, while the whole embryo surface was $S_{embryo} \simeq 4100\ \mu\text{m}^2$.

The probability of a microtubule to hit the cortex (Eq. 3 and 5) was modified as follow:

$$\tilde{\mathcal{M}}\left(\mathcal{S}, \alpha, \theta, \phi\right) = \frac{M}{4\pi} \frac{1}{1 + \alpha\, r_{\mathcal{S}}\left(\theta, \phi\right)} \frac{1}{r_{\mathcal{S}}\left(\theta, \phi\right)^2} \tag{14}$$

We then calculated the number of engaged force generators as above (Eq. 11) and found also a positional switch (Supplementary Fig. S4B compared to S4A). We concluded that this alternative modelling of force generator–microtubule attachment was compatible with the positional switch that we observed experimentally.

In contrast with the law of mass action in quantity, when the centrosome was further displaced towards the posterior after the positional switch, we did not observe any saturation in engaged force generators but a decrease (Fig. S4B). This may suggest that the centrosome position could control the oscillation die-down, if diffusion of member(s) of the trimeric complex in the cortex were the limiting factor. In such a case, one would expect that die-down did not intervene after a fixed delay from anaphase onset, but at a given position. This contrasted with experimental observations upon delaying anaphase onset (Table 1). Therefore, the law of mass action in quantity appeared to better model our data.

On top of this experimental argument, we estimated the lateral diffusion of the limited cortical anchors, likely GPR-1/2, and calculated a corresponding diffusion limited reaction rate equal to $k_{on}^{D} \simeq 1.2 \times 10^{5}$ s^{-1} after (Freeman and D., 1983; Freeman and Doll, 1983), considering the parameters detailed previously, a diffusion coefficient for GPR-1/2 similar to the one of PAR proteins $D = 0.2$ μm^2/s (Goehring et al., 2011), and a hydrodynamic radius of 5.2 nm (Erickson, 2009). Compared to the on-rate value proposed above (§2.2.3), i.e. $k_{on} \simeq 0.375$ s^{-1}, this suggested that lateral diffusion was not limiting. In contrast, it was proposed that in such a case, lateral diffusion may enhance rather than limit the reaction (Adam and Delbruck, 1968). We concluded that the process was limited by reaction, not diffusion, and we considered action mass in quantity (Eq. 9a) in the remaining of this work.

2.2.6 The processivity and microtubule dynamics set two independent switches on force generators: the expanded tug-of-war model

We next asked whether a cross-talk exists between the control of the oscillation onset by the processivity, as previously reported (Pecreaux et al., 2006), and the positional switch explained above. To do so, we let K_a varying with both the processivity $1/\overline{k_{off}}$ and the centrosome position. In the notations of the initial model, since we kept $\widehat{k_{on}}$ constant, it meant that k_{on} varied because of changes in the number of microtubule contacts in the posterior crescent, in turn depending on the centrosome position. We then found the pairs $(\overline{k_{off}^{c}}, x^{c})$ so that Eq. 6 was critical, i.e. $\Xi^{c} = \Gamma^{t}$ (Eq. 7), with x^{c} the critical position of the centrosome along the AP axis and $\overline{k_{off}^{c}}$ the critical off-rate. Because we considered the transverse axis and a single centrosome, we used $\Gamma^{t} = 140$ μN.s/m after (Garzon-Coral et al., 2016) and obtained the diagram reproduced in Fig. 2D that could be seen as a phase diagram. When the embryo trajectory (the orange arrow) crosses the first critical line (collection of $(\overline{k_{off}^{c}}, x^{c})$, depicted in blue) to go into the unstable region (blue area), the oscillations start and develop. Since this line is diagonal, it suggests that such an event depends upon the position of the posterior centrosome (ordinate axis) and the detachment rate (abscissa), suggesting that two control parameters contribute to making the system unstable and oscillating. Interestingly, when the embryo continues its trajectory in the phase diagram, it crosses the second critical line (depicted in green), which corresponds to the moment the system becomes stable again, and oscillations are damped out. This critical line is almost vertical indicating that this event depends mostly on the detachment rate, i.e. the inverse of processivity, consistent with the experimental observations (Table 1). Interestingly, this behaviour is maintained despite modest variations in the range of processivity and centrosome position explored during the division (i.e. the precise trajectory of the embryo in this phase diagram). Note that large values of detachment rate are irrelevant as they do not allow posterior displacement of the spindle (Fig. 5). We concluded that two independent switches control the onset of anaphase oscillations and broadly the burst of pulling forces contributing to spindle elongation and posterior displacement.

3 Simulating posterior displacement and final position

Because the cortical pulling forces involved in the anaphase spindle oscillations are also causing the posterior displacement, and because they depend on the position of the posterior centrosome, it creates a feedback loop on the posterior centrosome position. Resistance to changes of some parameters revealed by the sensitivity analysis of the oscillation onset suggests that these same parameters may have a reduced impact on the final position of the centrosome. In turn, this final position is essential as it contributes to determine the position of the cytokinesis cleavage furrow, a key aspect in an asymmetric division to correctly distribute cell fate determinants (Knoblich, 2010; Rappaport, 1971; White and Glotzer, 2012).

3.1 Modelling the posterior displacement of the spindle

To simulate the kinematics of posterior displacement, we considered the expanded model (§2.2) and a slowly-varying binding constant K_a due to the processivity increasing throughout mitosis (§2.2.3). We calculated the posterior pulling forces, assuming an axisymmetric distribution of force generators. The projection of the force exerted by the cortical pulling force generators implied a weakening factor because only the component parallel to the AP axis contributes to displace posteriorly the spindle. To calculate it, we made the assumption that any microtubule contacting the cortex in the active region has an equal probability to attach a force generator. Therefore, we obtained the force weakening due to AP axis projection by writing the ratio of the forces exerted by each microtubule contacting the cortex weighted by the probability of a contact and integrated over the active region, over the number of microtubule contacts calculated using Eq. 14. This weakening ratio was then multiplied by the number of bound force generators previously obtained (Eq. 11). The weakening of the pulling force along AP axis $\mathcal{F}$ then reads:

$$\mathcal{F}^{ante|post}\left(x, \overline{k_{off}}\right) = \frac{2\pi \int_{\theta=0}^{\theta_0^{ante|post}} p\left(\mathcal{S}, \alpha, x, \theta\right) \cos\theta \,\mathrm{d}\,\theta}{P\left(\mathcal{S}, \alpha, x\right)} \times \mathcal{N}\left(\mathcal{S}, \alpha, x, K_a^{ante|post}\right) \bar{f} \qquad (15)$$

with θ_0 the polar angle of the active region boundary positioned at x^0_{ante} and x^0_{post}, obtained assuming an ellipsoidal shape for the embryo. $p\left(\mathcal{S}, \alpha, x_{ante|post}, \theta\right)$ was defined at Eq. 3 and $P\left(\mathcal{S}, \alpha, x_{ante|post}\right)$ at Eq. 4. The Eq. 15 was used to calculate both anterior and posterior forces, with their respective parameters. After Rodriguez Garcia et al. (2017), the force asymmetry seemed to be due to an asymmetry of f.g.-MT affinity, under the control of GPR-1/2. We accounted for this asymmetric on-rate through an asymmetric attachment constant writing $K_a^{ante|post} = \beta^{ante|post} \widehat{kon} \,/\overline{k_{off}}$.

We put the above quantities into Eq 6 to finally get:

$$I^{post}\, \ddot{x}_{post} + \left(\Gamma - \Xi^{post}\right) \dot{x}_{post} + K\, x_{post} - K_{ante}\, x_{ante} = \eta + \mathcal{F}^{post}(x_{post}) - \mathcal{F}_{ante} \qquad (16)$$

with η a white noise modelling the force generator stochastic attachment and detachment (Nadrowski et al., 2004; Pecreaux et al., 2006). In particular, we used

$$k_{on} = \widehat{k_{on}} \left(\mathcal{M}\left(\mathcal{S}, \alpha, x_{post}\right) - \mathcal{N}\left(\mathcal{S}, \alpha, x_{post}, K_a^{post}\right)\right)$$

and also applied a weakening of anterior force to account for the uncoupling of spindle poles at anaphase onset (Maton et al., 2015; Mercat et al., 2017). We wrote:

$$F_{ante} = \begin{cases} \mathcal{F}_{ante} & \text{if} \quad \overline{k_{off}} \geq \overline{k^0_{off}} \\ \lambda \mathcal{F}_{ante} & \text{if} \quad \overline{k_{off}} < \overline{k^0_{off}} \end{cases} \tag{17a}$$

(17b)

Similarly, the centering force (Garzon-Coral et al., 2016; Pecreaux et al., 2016) was also weakened:

$$K_{ante} = \begin{cases} K & \text{if} \quad \overline{k_{off}} \geq \overline{k^0_{off}} \\ \lambda K & \text{if} \quad \overline{k_{off}} < \overline{k^0_{off}} \end{cases} \tag{18a}$$

(18b)

We solved this system numerically using trapezoidal rule and backward differentiation formula of order 2 (TR-BDF2 algorithm) (Hosea and Shampine, 1996). Since we linearised the equations and kept the anterior centrosome at a fixed position, we could explore only reasonable parameter variations when performing the final position parameter sensitivity analysis (Fig. 5, Supplementary Fig. S7). As a sanity check, we observed that modest variations in the force generator on-rate, thought to translate polarity cues (Rodriguez Garcia et al., 2017), modulated the final position as expected from experiments (Colombo et al., 2003; Grill et al., 2001). To ensure that our simulation correctly converged to the final position, we varied the spindle initial position and observed no significant change in the final position (Supplementary Fig. S7E).

3.2 Result and discussion: resistance of the final position to changes in force generator quantity and dynamics

We previously proposed that the final centrosome position was dictated both by the centering force stiffness and by the imbalance in pulling force generation, i.e. mainly the active force generator number in active region and their processivity (Pecreaux et al., 2006) (Fig. 5, Supplementary Fig. S7C-E dashed lines). In contrast, in the expanded model, when the posterior centrosome enters into the active region, more microtubules are oriented along the transverse axis than parallel to the AP axis (Fig. 2C *middle* and *right* panels) because of the isotropic distribution of the microtubules around the centrosome. Then, it limits the pulling forces on the posterior centrosome (Supplementary Fig. S7A). As a consequence, the boundary of the active region sets the final position (Supplementary Fig. S7B) as seen experimentally (Fig. 3A) and (Krueger et al., 2010). In contrast, the force generator quantity and dynamics become less important and the final position even shows some resistance to changes in these two parameters (Fig. 5, Supplementary Fig. S7C).

We noticed that when the active region boundary was located at 80% of embryo length or more posteriorly, and the spindle was close to the cell centre, the number of microtubules reaching this region was so reduced that it prevented a normal posterior displacement. Together with the observation that when the region extended more anteriorly the final position was anteriorly

shifted, it appeared that a boundary at 70% was a value quite optimal to maximise the posterior displacement. Because this posterior displacement is a key to asymmetric division, it would be interesting (but out of the scope of this work) to see whether a maximal posterior displacement is an evolutive advantage, which would then cause a pressure on the active region boundary.

4 Parameters used in modelling and simulations

In this section, we list the parameters used in calculating of the number of engaged force generators when validating the expanded tug-of-war model, and when simulating the posterior displacement. We based the parameter estimates on the initial model and on experiments performed elsewhere.

parameter	value	Description and estimate
	initial model parameters	
N	50 (38 for the initial model)	Number of force generators per half cortex (Grill et al., 2003) (identical on both sides (Rodriguez Garcia et al., 2017)). $N = 38$ when simulating the initial tug-of-war to ensure a similar posterior displacement as in expanded model, all other parameters remaining similar.
K	5 μN/m	Centering spring stiffness. Same order of magnitude as (Garzon-Coral et al., 2016; Pecreaux et al., 2006), although smaller since the AP axis is longer than the transverse axis, reducing centering stiffness (Howard, 2006).
k_{on}^{post}	3 s^{-1}	Fixed force generator attachment rate (on-rate) on posterior side, used only in initial model.
k_{on}^{ante}	2 s^{-1}	Fixed force generator attachment rate (on-rate) on anterior side, used only in initial model; its anterior value being lower than posterior to encode the polarity (Rodriguez Garcia et al., 2017).
x_{ante}	42%	Fixed anterior centrosome position (in % of embryo length), corresponding to experimental position at anaphase onset.
f_c	1.5 pN	Force generator detachment rate sensitivity to force (Pecreaux et al., 2006).
f'	3 μN.s/μm	Slope of the force generator force velocity relation (Pecreaux et al., 2006).
$\bar{f}$	6 pN	Force generator stall force (Pecreaux et al., 2006).
η	$\langle \lvert\eta\rvert \rangle = 0$ $\left\langle \lvert\eta\rvert^2 \right\rangle = 0.1\delta(t)$	Stochastic noise modelling the binding and unbinding of force generators.
	Expanded model	
a	24.6 μm	Embryo half-length (along AP axis), measured in this study.
b	15.75 μm	Embryo half-width (transverse to AP axis), measured in this study.
M	3000	Number of microtubules emanating from each centrosome (O'Toole et al., 2003; Redemann et al., 2016).
α	2.15 μm^{-1}	Microtubule dynamics parameter, corresponding to known growing/shrinking rates (Kozlowski et al., 2007; Srayko et al., 2005) and cortex residency time $\tau = 1.25$ s (this work and (Kozlowski et al., 2007)).
x_{post}^0	70%	Position of the boundary of the active region in posterior embryo half (in % of embryo length) (Krueger et al., 2010).

Simulating posterior displacement		
Γ	300 μN.s/m	Damping due to microtubule network (Howard, 2006) and cytoplasm viscosity (Garzon-Coral et al., 2016).
x^0_{ante}	40%	Position of the boundary of active force generator region in anterior embryo half (in % of embryo length). Assumed to correspond to LET-99 domain boundary (Krueger et al., 2010).
λ	0.5	Weakening factor of anterior forces to account for spindle pole uncoupling during elongation (Maton et al., 2015; Mercat et al., 2017).
$\overline{k^0_{off}}$	4 s^{-1}	Force generator off-rate at metaphase to anaphase transition, estimated from (Rodriguez Garcia et al., 2017).
$\overline{k^\infty_{off}}$	2 s^{-1}	Final force generator off-rate (Rodriguez Garcia et al., 2017).
$\overline{k^{init}_{off}}$	10 s^{-1}	Initial force generator off-rate. Time-dependent detachment rate (off-rate) $\overline{k_{off}}(t)$ varies following a sigmoid [2].
β_{post}	15	Affinity factor in posterior half of the cortex to account for the increased on-rate (Rodriguez Garcia et al., 2017). Set to have a number of active force generators in the range of 10 to 100 and twice larger in posterior than in anterior (Grill et al., 2003).
β_{ante}	7.5	Affinity factor in anterior half of the cortex to account for the increased on-rate (Rodriguez Garcia et al., 2017).
$\widehat{k_{on}}$	0.025 s^{-1}	Amplitude of the force generator attachment rate to the microtubule in the expanded model.

References

Adam, G. and Delbruck, M. (1968). Reduction of dimensionality in biological diffusion processes. In Structural Chemistry and Molecular Biology, (Rich, A., Davidson, N. and Pauling, L., eds), pp. 198–215. W. H. Freeman San Francisco.

Colombo, K., Grill, S. W., Kimple, R. J., Willard, F. S., Siderovski, D. P. and Gonczy, P. (2003). Translation of polarity cues into asymmetric spindle positioning in Caenorhabditis elegans embryos. Science *300*, 1957–61.

Edwards, J. (1892). An elementary treatise on the differential calculus, with applications and numerous examples. Macmillan and Co. The Macmillan Company, London, New York,.

Erickson, H. P. (2009). Size and shape of protein molecules at the nanometer level determined by sedimentation, gel filtration, and electron microscopy. Biol Proced Online *11*, 32–51.

Freeman, D. L. and D., D. J. (1983). The influence of diffusion on surface reaction kinetics. The Journal of Chemical Physics *78*, 6002.

[2] Equation reads $\overline{k_{off}}(t) = \overline{k^{init}_{off}} - (1 + \exp(-(t - t_{therm} - t_0)/T))^{-1} \times K_{off}$, with t the time, $t_{therm} = 50$ s the thermalisation time, $t_0 = 175$ s the transition time, $T = 70$ s the time width and $K_{off} = \overline{k^{init}_{off}} - \overline{k^\infty_{off}}$ s^{-1} the variation amplitude.

Freeman, D. L. and Doll, J. D. (1983). Langevin analysis of the diffusion model for surface chemical reactions. The Journal of Chemical Physics *79*, 2343.

Garzon-Coral, C., Fantana, H. A. and Howard, J. (2016). A force-generating machinery maintains the spindle at the cell center during mitosis. Science *352*, 1124–7.

Goehring, N. W., Hoege, C., Grill, S. W. and Hyman, A. A. (2011). PAR proteins diffuse freely across the anterior-posterior boundary in polarized C. elegans embryos. J Cell Biol *193*, 583–94.

Grill, S. W., Gonczy, P., Stelzer, E. H. and Hyman, A. A. (2001). Polarity controls forces governing asymmetric spindle positioning in the Caenorhabditis elegans embryo. Nature *409*, 630–3.

Grill, S. W., Howard, J., Schaffer, E., Stelzer, E. H. and Hyman, A. A. (2003). The distribution of active force generators controls mitotic spindle position. Science *301*, 518–21.

Grill, S. W., Kruse, K. and Julicher, F. (2005). Theory of mitotic spindle oscillations. Physical Review Letters *94*, 108104.

Hosea, M. E. and Shampine, L. F. (1996). Analysis and implementation of TR-BDF2. Applied Numerical Mathematics *20*, 21–37.

Howard, J. (2006). Elastic and damping forces generated by confined arrays of dynamic microtubules. Physical biology *3*, 54–66.

Knoblich, J. A. (2010). Asymmetric cell division: recent developments and their implications for tumour biology. Nat Rev Mol Cell Biol *11*, 849–60.

Koonce, M. P. and Tikhonenko, I. (2012). Dynein Motor Mechanisms. In Dyneins : structure, biology and disease, (King, S. M., ed.), pp. xv, 639 p. Academic Press Amsterdam ; Boston 1st edition.

Kozlowski, C., Srayko, M. and Nedelec, F. (2007). Cortical microtubule contacts position the spindle in C. elegans embryos. Cell *129*, 499–510.

Krueger, L. E., Wu, J. C., Tsou, M. F. and Rose, L. S. (2010). LET-99 inhibits lateral posterior pulling forces during asymmetric spindle elongation in C. elegans embryos. J Cell Biol *189*, 481–95.

Maton, G., Edwards, F., Lacroix, B., Stefanutti, M., Laband, K., Lieury, T., Kim, T., Espeut, J., Canman, J. C. and Dumont, J. (2015). Kinetochore components are required for central spindle assembly. Nat Cell Biol *17*, 697–705.

Mercat, B., Pinson, X., Le Cunff, Y., Fouchard, J., Mary, H., Pastezeur, S., Gachet, Y., Tournier, S., Bouvrais, H. and Pecreaux, J. (2017). Micro-fluctuations of spindle length reveal its dynamics over cell division. (in preparation).

Nadrowski, B., Martin, P. and Julicher, F. (2004). Active hair-bundle motility harnesses noise to operate near an optimum of mechanosensitivity. Proc Natl Acad Sci U S A *101*, 12195–200.

Nguyen-Ngoc, T., Afshar, K. and Gonczy, P. (2007). Coupling of cortical dynein and G alpha proteins mediates spindle positioning in Caenorhabditis elegans. Nature Cell Biology *9*, 1294–1302.

O'Toole, E. T., McDonald, K. L., Mantler, J., McIntosh, J. R., Hyman, A. A. and Muller-Reichert, T. (2003). Morphologically distinct microtubule ends in the mitotic centrosome of Caenorhabditis elegans. J Cell Biol *163*, 451–6.

Park, D. H. and Rose, L. S. (2008). Dynamic localization of LIN-5 and GPR-1/2 to cortical force generation domains during spindle positioning. Developmental Biology *315*, 42–54.

Pecreaux, J., Redemann, S., Alayan, Z., Mercat, B., Pastezeur, S., Garzon-Coral, C., Hyman, A. A. and Howard, J. (2016). The Mitotic Spindle in the One-Cell C. elegans Embryo Is Positioned with High Precision and Stability. Biophys J *111*, 1773–1784.

Pecreaux, J., Roper, J. C., Kruse, K., Julicher, F., Hyman, A. A., Grill, S. W. and Howard, J. (2006). Spindle oscillations during asymmetric cell division require a threshold number of active cortical force generators. Current Biology *16*, 2111–22.

Rappaport, R. (1971). Cytokinesis in animal cells. Int Rev Cytol *31*, 169–213.

Redemann, S., Baumgart, J., Lindow, N., Fuerthauer, S., Nazockdast, E., Kratz, A., Prohaska, S., Brugues, J., Shelley, M. and Mueller-Reichert, T. (2016). Kinetochore Microtubules indirectly link Chromosomes and Centrosomes in C. elegans Mitosis. BioRxiv *060855*.

Riche, S., Zouak, M., Argoul, F., Arneodo, A., Pecreaux, J. and Delattre, M. (2013). Evolutionary comparisons reveal a positional switch for spindle pole oscillations in Caenorhabditis embryos. Journal of Cell Biology *201*, 653–62.

Rodriguez Garcia, R., Chesneau, L., Pastezeur, S., Roul, J., Tramier, M. and Pecreaux, J. (2017). Dynamics of dynein at microtubule plus-ends and the cortex during the division of the C. elegans zygote. bioRxiv preprint , 118604.

Srayko, M., Kaya, A., Stamford, J. and Hyman, A. A. (2005). Identification and characterization of factors required for microtubule growth and nucleation in the early C. elegans embryo. Dev Cell *9*, 223–36.

White, E. A. and Glotzer, M. (2012). Centralspindlin: At the heart of cytokinesis. Cytoskeleton (Hoboken) *69*, 882–92.